Outage Analysis in MIMO Free-Space Optical Channels with Pulse-Position Modulation

N. Letzepis and A. Guillén i Fàbregas

CUED / F-INFENG / TR 597
February 2008

Outage Analysis in MIMO Free-Space Optical Channels with Pulse-Position Modulation

Nick Letzepis and Albert Guillén i Fàbregas

Abstract

Free space optical communication is an attractive alternative to radio frequency for the purpose of transmitting data on the order of gigabits per second. The main drawback in communicating via the free space optical channel is the detrimental effect the atmosphere has on a propagating laser beam. Atmospheric turbulence causes random fluctuations in the irradiance of the received optical laser beam, commonly referred to as *scintillation*. The scintillation process is slow compared to the large data rates typical of optical transmission. As such, we adopt a quasi-static block fading model and study the outage probability of the channel under the assumption of orthogonal pulse-position modulation. We investigate the mitigation of scintillation through the use of multiple lasers and multiple apertures, thereby creating a multiple-input multiple output (MIMO) channel. Non-ideal photodetection is also assumed such that the combined shot noise and thermal noise are considered as signal-independent additive Gaussian white noise. Assuming perfect receiver channel state information (CSI), we compute the signal-to-noise ratio exponents for the cases when the scintillation is lognormal, exponential, gamma-gamma and lognormal-Rice distributed, which cover a wide range of atmospheric turbulence conditions. Furthermore, we illustrate very large gains, in some cases larger than 20 dB, when transmitter CSI is also available by adapting the transmitted electrical power.

N. Letzepis is with Institute for Telecommunications Research, University of South Australia, SPRI Building - Mawson Lakes Blvd., Mawson Lakes SA 5095, Australia, e-mail: nick.letzepis@unisa.edu.au.

A. Guillén i Fàbregas is with the Department of Engineering, University of Cambridge, Cambridge CB2 1PZ, UK, e-mail: guillen@ieee.org.

I. Introduction

Free space optical (FSO) communication offers an attractive alternative to the radio frequency (RF) channel for the purpose of transmitting data at very high rates. By utilising a high carrier frequency in the optical range, digital communication on the order of gigabits per second is possible. In addition, FSO links are difficult to intercept, immune to interference or jamming from external sources, and are not subject to frequency spectrum regulations. FSO communications have received recent attention in applications such as satellite communications, fiber-backup, RF-wireless back-haul and last-mile connectivity [1].

The main drawback of the FSO channel is the detrimental effect the atmosphere has on a propagating laser beam. The atmosphere is composed of gas molecules, water vapor, pollutants, dust, and other chemical particulates that are trapped by Earth's gravitational field. Since the wavelength of a typical optical carrier is comparable to these molecule and particle sizes, the carrier wave is subject to various propagation effects that are uncommon to RF systems. One such effect is *scintillation*, caused by atmospheric turbulence, and refers to random fluctuations in the irradiance of the received optical laser beam (analogous to fading in RF systems) [2–4].

Recent works on the mitigation of scintillation concentrate on the use of multiple-lasers and multiple-apertures to create a multiple-input-multiple-output (MIMO) channel [5–13]. Many of these works consider scintillation as an ergodic fading process, and analyse the channel in terms of its ergodic capacity. However, compared to typical data rates, scintillation is a slow time-varying process (with a coherence time on the order of milliseconds), and it is therefore more appropriate to analyse the outage probability of the channel. To some extent, this has been done in the works of [6, 10, 12–14]. In [6, 13] the outage probability of the MIMO FSO channel is analysed under the assumption of ideal photodetection (PD) (i.e. PD is modeled as a Poisson counting process) with no bandwidth constraints. Wilson *et al.* [10] also assume perfect PD, but with the further constraint of pulse-position modulation (PPM). Lee and Chan [12], study the outage probability under the assumption of on-off keying (OOK) transmission and non-ideal PD, i.e. the combined shot noise and thermal noise process is modeled as zero mean signal independent additive white Gaussian noise (AWGN). Farid and Hranilovic [14] extend this analysis to include the effects of pointing errors.

In this report we study the outage probability of the MIMO FSO channel under the assumptions of PPM, non-ideal PD, and equal gain combining (EGC) at the receiver. In particular, we model the channel as a quasi-static block fading channel whereby communication takes place over a finite number of blocks and each block of transmitted symbols experiences an independent identically distributed (i.i.d.) fading realisation [15, 16]. Given the slow time-varying nature of scintillation, channel state information (CSI) can be estimated at the receiver and fed back to the transmitter via a dedicated feedback link. We consider two types of CSI knowledge. First we assume perfect CSI is available only at the receiver (CSIR case), and the transmitter knows only the channel statistics. We study a number of scintillation distributions, i.e., lognormal, modelling weak turbulence; exponential, modelling strong turbulence; gamma-gamma [17] and lognormal-Rice [18, 19], modelling a wide range of turbulence conditions. For the CSIR-only case, we derive signal-to-noise ratio (SNR) exponents and show that these exponents are composed of a channel related parameter (dependent on the scintillation distribution) times the Singleton bound [20–22]. Then we consider the case when perfect CSI is known at both the transmitter and receiver (CSIT case). For this case, the transmitter finds the optimal power allocation to minimise the outage probability [23]. Using results from [24], we derive the optimal power allocation that minimises the outage probability, subject to short- and long-term power constraints. We show that under a long-term power constraint, very large power savings can be achieved, and that the delay-limited capacity [25] always exists for lognormal distributed scintillation, whereas, for the exponential, gamma-gamma and lognormal-Rice cases, one must code over several blocks for delay-limited capacity to exist. The number of required blocks depends on the rate of the binary code via the SNR exponent. We show that with the use of MIMO one needs only to code over a single realisation to ensure the existance of delay-limited capacity. These results highlight the benefits of MIMO and block diversity in reducing the outage probability in FSO systems.

The report is organised as follows. In Section II, we define the channel model and assumptions. In Section III we review the lognormal, exponential, gamma-gamma and lognormal-Rice scintillation models. Section IV defines the outage probability and presents results on the minimum-mean squared error (MMSE). Then in Sections V and VI we present the main results of our asymptotic outage probability analysis for the CSIR and CSIT cases, respectively. Concluding remarks are then given in Section VII. Proofs of the various results can be found in the Appendices.

II. System Model

We consider an FSO system with M transmit lasers an N aperture receiver as shown in Figure 1. Information data is first encoded by a binary code of rate R_c. The encoded stream is modulated according to a Q-ary PPM scheme, resulting in rate $R = R_c \log_2 Q$ (bits/channel use). Repetition transmission is employed such that the same PPM signal is transmitted in perfect synchronism by each of the M lasers through an atmospheric turbulent channel and collected by N receive apertures. We assume the distance between the individual lasers and apertures is sufficient so that spatial correlation is negligible. At each aperture, the received optical signal is converted to an electrical signal via PD. Non-ideal PD is assumed such that the combined shot noise and thermal noise processes can be modeled as zero mean, signal independent AWGN (an assumption commonly used in the literature, see e.g. [3–5, 12, 14, 26–31]).

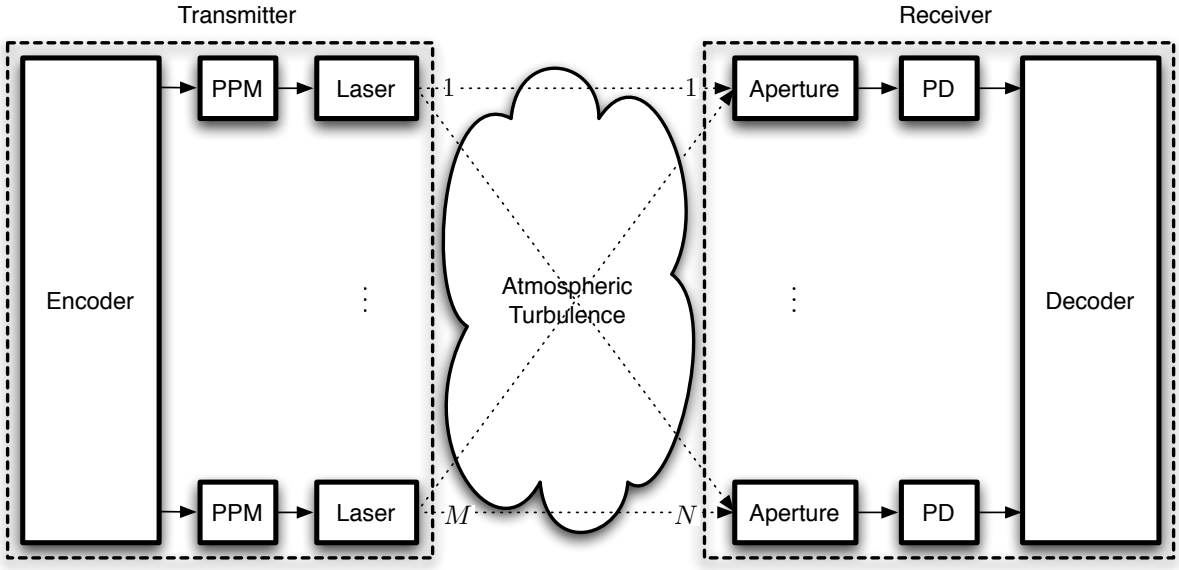

Fig. 1. Block diagram of an FSO MIMO system.

In FSO communications, channel variations are typically much slower than the signaling period. As such, we model the channel as a non-ergodic block-fading channel, for which a given codeword of length BL undergoes only a finite number B of scintillation realisations [15, 16]. The received signal at aperture $1 \leq n \leq N$ can be written as

$$\boldsymbol{y}_b^n[\ell] = \left(\sum_{m=1}^{M} \tilde{h}_b^{m,n} \right) \sqrt{\tilde{p}_b}\, \boldsymbol{x}_b[\ell] + \tilde{\boldsymbol{z}}_b^n[\ell], \tag{1}$$

for $b = 1, \ldots, B, \ell = 1, \ldots, L$, where $\boldsymbol{y}_b^n[\ell], \tilde{\boldsymbol{z}}_b^n[\ell] \in \mathbb{R}^Q$ are the received and noise signals at block b, time instant ℓ and aperture n, $\boldsymbol{x}_b[\ell], \in \mathbb{R}^Q$ is the transmitted signal at block b and time instant ℓ, and $\tilde{h}_b^{m,n}$ denotes the scintillation fading coefficient between laser m and aperture n. Each transmitted symbol is drawn from a PPM alphabet, $\boldsymbol{x}_b[\ell] \in \mathcal{X}^{\text{ppm}} \triangleq \{\boldsymbol{e}_1, \ldots, \boldsymbol{e}_Q\}$, where $\boldsymbol{e}_q$ is the canonical basis vector,

i.e., it has all zeros except for a one in position q, the time slot where the pulse is transmitted. The noise samples of $\tilde{\boldsymbol{z}}_b^n[\ell]$ are independent realisations of a random variable $Z \sim \mathcal{N}(0,1)$, and $\tilde{p}_b$ denotes the received electrical power of block b at each aperture in the absence of scintillation. The fading coefficients $\tilde{h}_b^{m,n}$ are independent realisations of a random variable $\tilde{H}$ with probability density function (pdf) $f_{\tilde{H}}(h)$.

At the receiver, we assume equal gain combining (EGC) is employed, such that

$$\boldsymbol{y}_b[\ell] = \frac{1}{\sqrt{N}} \sum_{n=1}^{N} \boldsymbol{y}_b^n[\ell] \tag{2}$$

$$= \frac{1}{\sqrt{N}} \sum_{n=1}^{N} \sum_{m=1}^{M} \tilde{h}_b^{m,n} \sqrt{\tilde{p}_b} \boldsymbol{x}_b[\ell] + \frac{1}{\sqrt{N}} \sum_{n=1}^{N} \tilde{\boldsymbol{z}}_b^n[\ell] \tag{3}$$

$$= M\sqrt{N\tilde{p}_b}\ \hat{h}_b\ \boldsymbol{x}_b[\ell] + \boldsymbol{z}_b[\ell], \tag{4}$$

where

$$\hat{h}_b = \frac{1}{MN} \sum_{m=1}^{M} \sum_{n=1}^{N} \tilde{h}_b^{m,n} \tag{5}$$

and

$$\boldsymbol{z}_b[\ell] = \frac{1}{\sqrt{N}} \sum_{n=1}^{N} \tilde{\boldsymbol{z}}_b^n[\ell] \sim \mathcal{N}(0,1). \tag{6}$$

Letting $h_b \triangleq \hat{h}_b / \sqrt{\mathbb{E}[\hat{h}_b^2]}$ gives

$$\boldsymbol{y}_b[\ell] = \sqrt{p_b} h_b \boldsymbol{x}_b[\ell] + \boldsymbol{z}_b[\ell], \tag{7}$$

where

$$p_b = M^2 N \mathbb{E}[\hat{h}_b^2] \tilde{p}_b. \tag{8}$$

Hence (7) can be considered as a SISO channel with an *equivalent* fading coefficient h_b, normalized such that $\mathbb{E}[H^2] = 1$.[1]Thus, the average received electrical SNR can be expressed as $\mathsf{snr} \triangleq \mathbb{E}[p h_b^2] = \mathbb{E}[p_b]$.

We will consider two cases of channel state information (CSI). We will first study the case of perfect CSIR, and we will then consider the case of perfect CSIT as well as CSIR. In the case where we have only CSIR, we will distribute the electrical power uniformly over the blocks, i.e., $p_b = p = \mathsf{snr}$ for $b = 1, \ldots, B$. Otherwise, in the case of CSIT, we will allocate electrical power in order to improve performance. In particular, in the case of perfect CSIR and CSIT, we will consider the following two electrical power constraints

$$\text{Short-term:} \quad \frac{1}{B} \sum_{b=1}^{B} p_b \leq P \tag{9}$$

$$\text{Long-term:} \quad \mathbb{E}\left[\frac{1}{B} \sum_{b=1}^{B} p_b\right] \leq P. \tag{10}$$

Throughout the report, we will devote special attention to the case of $B = 1$, i.e., the channel does not vary within a codeword. This scenario is relevant for FSO, since, due to the large data-rates, one is able to transmit millions of bits virtually over the same channel realisation. We will see that most results admit very simple forms, and some times, even closed form. This analysis allows for a system characterisation where the expressions highlight the roles of the key design parameters.

[1]For ideal PD, the normalisation $\mathbb{E}[H] = 1$ is used to keep optical power constant. We assume non-ideal PD and work entirely in the electrical domain. Hence, we chose the normalisation $\mathbb{E}[H^2] = 1$, used commonly in RF fading channels. Since we consider only the asymptotic behaviour of the outage probability, the specific normalisation is irrelevant and does not affect our results.

III. Scintillation Distributions

The scintillation pdf, $f_{\tilde{H}}(h)$, is parameterised by the *scintillation index* (SI),

$$\sigma_I^2 \triangleq \frac{\mathrm{Var}(\tilde{H})}{(\mathbb{E}[\tilde{H}])^2}. \tag{11}$$

Under weak atmospheric turbulence conditions (defined as those regimes for which $\sigma_I^2 < 1$), the SI is proportional to the so called *Rytov variance* which represents the SI of an unbounded plane wave in weak turbulence conditions, and is also considered as a measure of the strength of the optical turbulence under strong-fluctuation regimes [4]. As the Rytov variance increases, the SI continues to increase beyond the weak turbulence regime until it reaches a maximum value greater than unity. At that point the SI begins to decrease with increasing Rytov variance and approaches unity from above. This region is termed the *saturation region* [17, 32].

The distribution of the irradiance fluctuations is dependent on the strength of the optical turbulence. For the weak turbulence regime, the fluctuations are generally considered to be lognormally distributed, and for very strong turbulence, exponentially distributed [2, 33]. For moderate turbulence, the distribution of the fluctuations is not well understood, and a number of distributions have been proposed, such as the lognormal-Rice distribution [4, 17, 19, 34, 35] (also known as the Beckmann distribution [36]) and K-distribution [34]. In [17], Al-Habash *et al.* proposed a gamma-gamma distribution as a general model for all levels of atmospheric turbulence. Moreover, recent work in [35] has shown that the gamma-gamma model is in close agreement with experimental measurements under moderate-to-strong turbulence conditions. In this report we focus on lognormal, exponential, gamma-gamma and lognormal-Rice distributed scintillation.

For MIMO-EGC FSO communication systems, $\hat{h}_b$ and h_b are realisations of random variables $\hat{H}$ and H respectively, which are functions of $\tilde{h}_b^{m,n}$ for $m = 1, \ldots, M$ and $n = 1, \ldots, N$. In (8) we can determine $\mathbb{E}[\hat{H}^2]$ in terms of the scintillation index,

$$\mathbb{E}[\hat{H}^2] = \frac{\mathbb{E}[\tilde{H}^2]}{MN} + \frac{(MN-1)}{MN}\mathbb{E}[\tilde{H}]^2 = \mathbb{E}[\tilde{H}]^2\left(1 + \frac{\sigma_I^2}{MN}\right) \tag{12}$$

Hence the mean and variance of H is therefore

$$\mathbb{E}[H] = \frac{\mathbb{E}[\tilde{H}]}{\sqrt{\mathbb{E}[\hat{H}^2]}} = \frac{1}{\sqrt{1 + \frac{\sigma_I^2}{MN}}}. \tag{13}$$

$$\mathrm{var}[H] = \mathbb{E}[H^2] - \mathbb{E}[H]^2 = 1 - \frac{1}{1 + \frac{\sigma_I^2}{MN}}. \tag{14}$$

A. Lognormal Scintillation

For *lognormal distributed scintillation*,

$$f_{\tilde{H}}(h) = \frac{1}{h\tilde{\sigma}\sqrt{2\pi}} \exp\left(-(\log h - \tilde{\mu})^2/(2\tilde{\sigma}^2)\right), \tag{15}$$

where $\tilde{\mu}$ and $\tilde{\sigma}$ are related to the SI via $\tilde{\mu} = -\log(1+\sigma_I^2)$ and $\tilde{\sigma}^2 = \log(1+\sigma_I^2)$. The distribution of H results from a summation of MN lognormal distributions, for which the pdf is unknown. However, it is well known that the distribution resulting from the sum of independent lognormal random variables can be accurately approximated by a lognormal distribution [37–40], i.e.

$$f_H(h) \approx \frac{1}{h\sigma\sqrt{2\pi}} \exp\left(-(\log h - \mu)^2/(2\sigma^2)\right), \tag{16}$$

where from (13) and (14) we have

$$\mu = -\log\left(1 + \frac{\sigma_I^2}{MN}\right) \tag{17}$$

$$\sigma^2 = \log\left(1 + \frac{\sigma_I^2}{MN}\right). \tag{18}$$

Thus as $M, N \to \infty$, $\mu, \sigma^2 \to 0$ and the distribution becomes more concentrated about a mean of 1, i.e. the system approaches the non-fading channel.

The distribution of H can also be computed numerically by performing an $(MN-1)$-fold convolution or via a fast Fourier transform (FFT) method. The later approach, being less computationally expensive, involves performing the FFT of a truncated lognormal distribution, raising it to the MNth power and then computing the inverse-FFT (IFFT) (details are given in Appendix I). The accuracy of the FFT method depends both on the truncation and the length of the FFT. Fig. 2 compares the PDF of H computed numerically using the FFT method (with $h_{\max} = 64$ and $N_{\text{FFT}} = 2^{21}$) to the log-normal approximation. It can be seen that the lognormal approximation is quite a good fit except for the right hand side tail, for which the approximation tends to over-estimate.

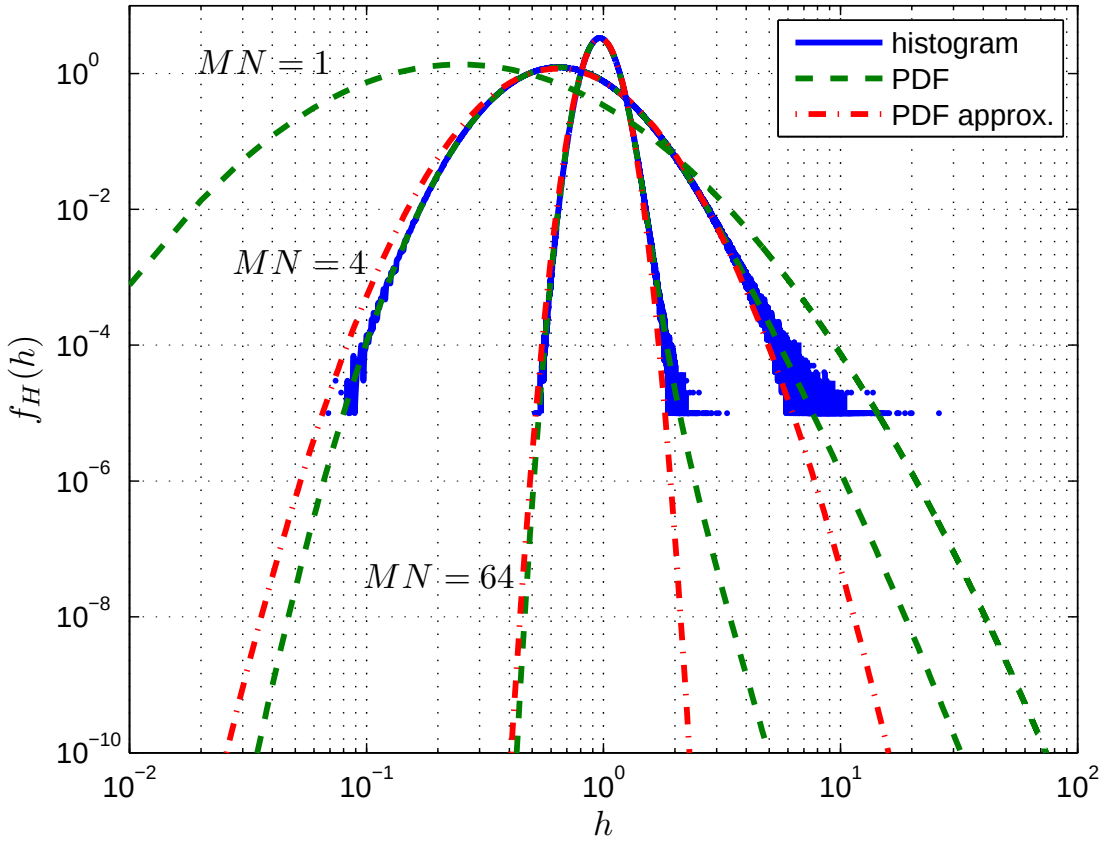

Fig. 2. PDF of H when $\tilde{H}$ is a lognormal random variable with $\sigma_I^2 = 1$: solid line shows simulation results; dashed line shows PDF computed numerically via FFT method and the dot-dashed line shows the lognormal approximation (16).

B. Exponential Scintillation

For *exponential distributed scintillation*,

$$f_{\tilde{H}}(h) = \lambda \exp(-\lambda h). \tag{19}$$

Note that this corresponds to the super-saturated turbulence regime, for which $\sigma_I^2 = 1$. We may also interpret $\tilde{H}$ as a Gamma distributed random variable, since $f_{\tilde{H}}(h) = g(h; 1, 1/\lambda)$ where [41, Ch. 17]

$$g(h; k, \theta) = h^{k-1} \frac{\exp(-h/\theta)}{\theta^k \Gamma(k)}. \tag{20}$$

Since sums of Gamma distributed random variables are also Gamma distributed [41, Ch. 17] we have,

$$f_{\hat{H}}(h) = g\left(h; MN; \frac{1}{\lambda MN}\right) \tag{21}$$

and

$$\mathbb{E}[\hat{H}^2] = \frac{1}{\lambda^2}\left(1 + \frac{1}{MN}\right). \tag{22}$$

The normalized combined fading coefficient is

$$f_H(h) = g\left(h; MN; (MN(1+MN))^{-\frac{1}{2}}\right), \tag{23}$$

which is independent of λ. Fig. 3 plots (23) for $MN = 1, 4, 64$.

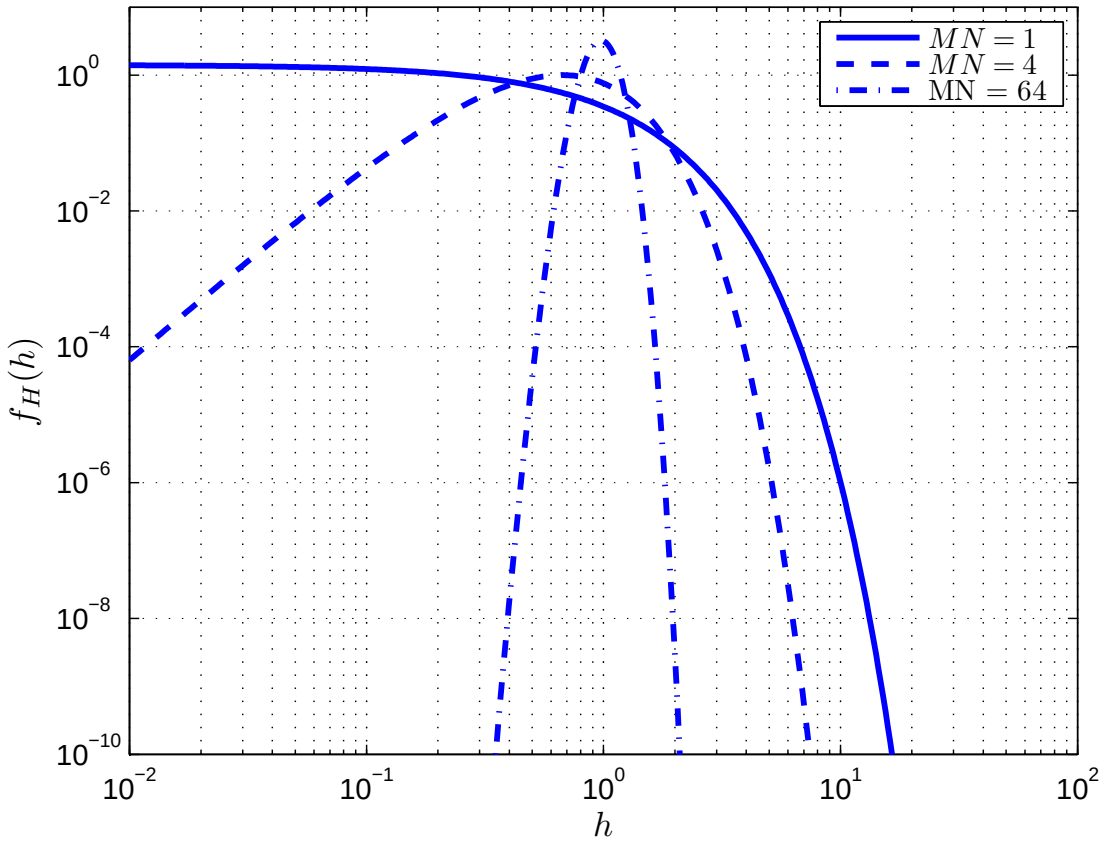

Fig. 3. PDF of H when $\tilde{H}$ is exponential distributed (23).

C. Gamma-Gamma Scintillation

The *gamma-gamma distribution* arises from the product of two independent Gamma distributed random variables and [17],

$$f_{\tilde{H}}(h) = \frac{2(\alpha\beta)^{\frac{\alpha+\beta}{2}}}{\Gamma(\alpha)\Gamma(\beta)} h^{\frac{\alpha+\beta}{2}-1} \mathrm{K}_{\alpha-\beta}(2\sqrt{\alpha\beta h}), \tag{24}$$

where $\mathrm{K}_\nu(x)$ denotes the modified Bessel function of the second kind. The parameters α and β are related with the scintillation index via $\sigma_I^2 = \alpha^{-1} + \beta^{-1} + (\alpha\beta)^{-1}$.

The moments of h can be determined via

$$\mathbb{E}[\tilde{H}^k] = \frac{\Gamma(\alpha+k)\Gamma(\beta+k)}{\Gamma(\alpha)\Gamma(\beta)} (\alpha\beta)^{-k}, \tag{25}$$

or recursively using

$$\mathbb{E}[\tilde{H}^k] = \mathbb{E}[\tilde{H}^{k-1}](k-1+\alpha)(k-1+\beta)(\alpha\beta)^{-1}. \tag{26}$$

Hence, $\mathbb{E}[\tilde{H}] = 1$ and $\mathbb{E}[\tilde{H}^2] = 1/(1+\sigma_I^2)$.

Unfortunately, finding a closed form expression for the distribution resulting from sums of Gamma-Gamma distributed random variables is difficult. We can however obtain the moment generating function (MGF) from which we can obtain the distribution of H via the inverse Fourier transform. First consider the following theorem..

Theorem 3.1: The moment generating function (MGF) of the Gamma-Gamma distribution (24) is given by

$$M_{\tilde{H}}(t) = {}_2\mathrm{F}_0(\alpha, \beta; t/(\alpha\beta)), \tag{27}$$

for $t < 0$, where ${}_2\mathrm{F}_0$ denotes the generalized hypergeometric function.

Proof: See Appendix II-A. ■

Note that the hypergeometric function (27) may also be written as [42, Ch. 13]

$${}_2\mathrm{F}_0(\alpha, \beta; t/(\alpha\beta)) = \left(-\frac{\alpha\beta}{t}\right)^{\alpha} U\left(\alpha, 1+\alpha-\beta, -\frac{\alpha\beta}{t}\right),$$

where $U(a,b,z) = \frac{1}{\Gamma(a)}\int_0^\infty e^{-zt}(t-1)^{a-1}t^{b-a-1}\,dt$. Furthermore, for the special case, $\beta = 1$ corresponding to K-distributed scintillation [4, Sec. 9.9.1], we have

$${}_2\mathrm{F}_0(\alpha, 1; t/\alpha) = \exp\left(-\frac{\alpha}{t}\right)\left(-\frac{\alpha}{t}\right)^{\alpha}\Gamma\left(1-\alpha, -\frac{\alpha}{t}\right),$$

where $\Gamma(a,x) \triangleq \int_x^\infty t^{a-1}\exp(-t)dt$ denotes the upper incomplete gamma function [42, p.260].

Setting $t = j\omega$ in (27), one obtains the *characteristic function*. The characteristic function of a sum of independent random variables is equal to the multiplication of their respective characteristic functions [43]. Hence, by taking the inverse Fourier transform, the pdf of $\hat{H}$ and H are respectively

$$f_{\hat{H}}(h) = \frac{MN}{2\pi}\int_{-\infty}^{\infty} [{}_2\mathrm{F}_0(\alpha, \beta; j\omega/(\alpha\beta))]^{MN} \exp\left(-j\omega MNh\right) d\omega, \tag{28}$$

$$f_H(h) = \left[1 + \frac{\sigma_I^2}{MN}\right]^{\frac{1}{2}} f_{\hat{H}}\left(\left[1+\frac{\sigma_I^2}{MN}\right]^{\frac{1}{2}} h\right). \tag{29}$$

In addition to (29) we may also compute the PDF of H using the FFT method (as in the case for lognormal $\tilde{H}$). The FFT method turns out to be much faster than performing the integration (29) numerically. Fig. 4 compares the PDF of H using the FFT method (dashed line) to histograms of 10^8 i.i.d. samples from H (solid).

From [4, 17] the gamma-gamma cdf is given by:

$$\begin{aligned} F_{\tilde{H}}(h) =& \frac{(\alpha\beta h)^{\alpha}\Gamma(\beta-\alpha)}{\alpha\Gamma(\alpha)\Gamma(\beta)} {}_1\mathrm{F}_2(\alpha; 1+\alpha, 1+\alpha-\beta; \alpha\beta h) \\ &+ \frac{(\alpha\beta h)^{\beta}\Gamma(\alpha-\beta)}{\beta\Gamma(\alpha)\Gamma(\beta)} {}_1\mathrm{F}_2(\beta; 1+\beta, 1+\beta-\alpha; \alpha\beta h) \end{aligned} \tag{30}$$

Note (30) is not valid when $\alpha = \beta$, or when $|\alpha - \beta|$ is an integer. However, for small h, we can circumvent this problem by using the following approximation.

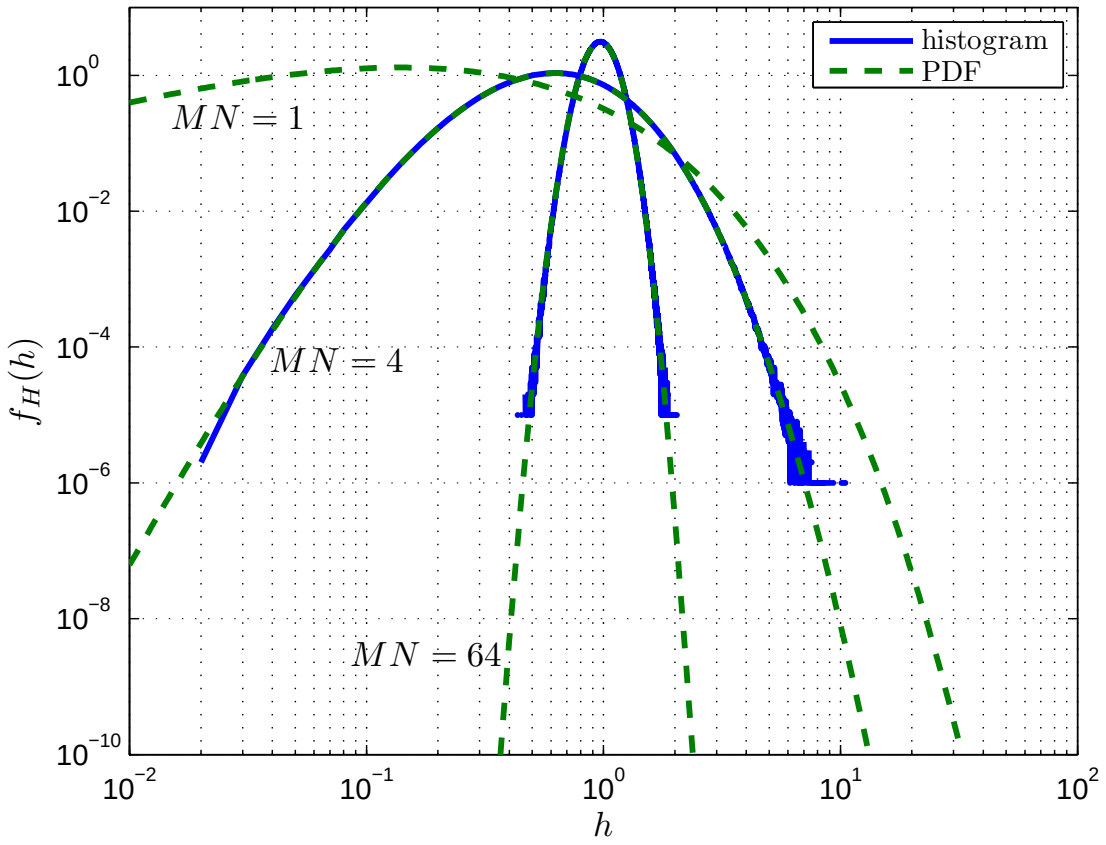

Fig. 4. PDF of H when $\tilde{H}$ is Gamma-Gamma distributed with $\alpha = 2.05$ and $\beta = 2.45$: solid lines, histogram of randomly generated samples; dashed lines, numerical computation using the FFT method.

Proposition 3.1: For small h the cdf of a gamma-gamma distributed random variable can be approximated as

$$F_{\tilde{H}}(h) \approx \begin{cases} \frac{\alpha^{2(\alpha-1)}}{(\Gamma(\alpha))^2}\left[1 + 2\alpha \log \frac{1}{2\alpha} + \alpha \log \frac{1}{h}\right] h^{\alpha}, & \beta = \alpha \\ \frac{\Gamma(|\alpha-\beta|)}{\Gamma(\alpha)\Gamma(\beta)} \frac{(\alpha\beta h)^{\min(\alpha,\beta)}}{\min(\alpha,\beta)}, & \beta \neq \alpha \end{cases} \tag{31}$$

Proof: See Appendix II-B. ■

Fig. 5 illustrates the convergence of (31) to (30) as h decreases. This figure shows that the approximation is tight as $h \to 0$.

D. Lognormal-Rice Scintillation

For the lognormal-Rice distribution, like the gamma-gamma case, the fading random variable is written as the product of two independent random variables, $\tilde{H} = XY$, where X is a lognormal distributed random variable with parameters σ^2 and $\mu = -\sigma^2/2$, and $\sqrt{Y}$ Rice distributed random variable, i.e.

$$f_{\sqrt{Y}}(y) = \frac{y}{\sigma_R^2} \exp\left(-\frac{y^2 + \nu_R^2}{2\sigma_R^2}\right) I_0\left(\frac{y\nu_R}{\sigma_R^2},\right) \tag{32}$$

where $I_0(z)$ denotes the modified Bessel function of the first kind, and the parameters of the distribution are set to

$$\sigma_R^2 = \frac{1}{2(r+1)}, \qquad \nu_R = \sqrt{\frac{r}{r+1}}. \tag{33}$$

Hence the pdf of Y is

$$f_Y(y) = (r+1)\exp(-r-(r+1)y) I_0\left(\sqrt{4r(r+1)y}\right) \tag{34}$$

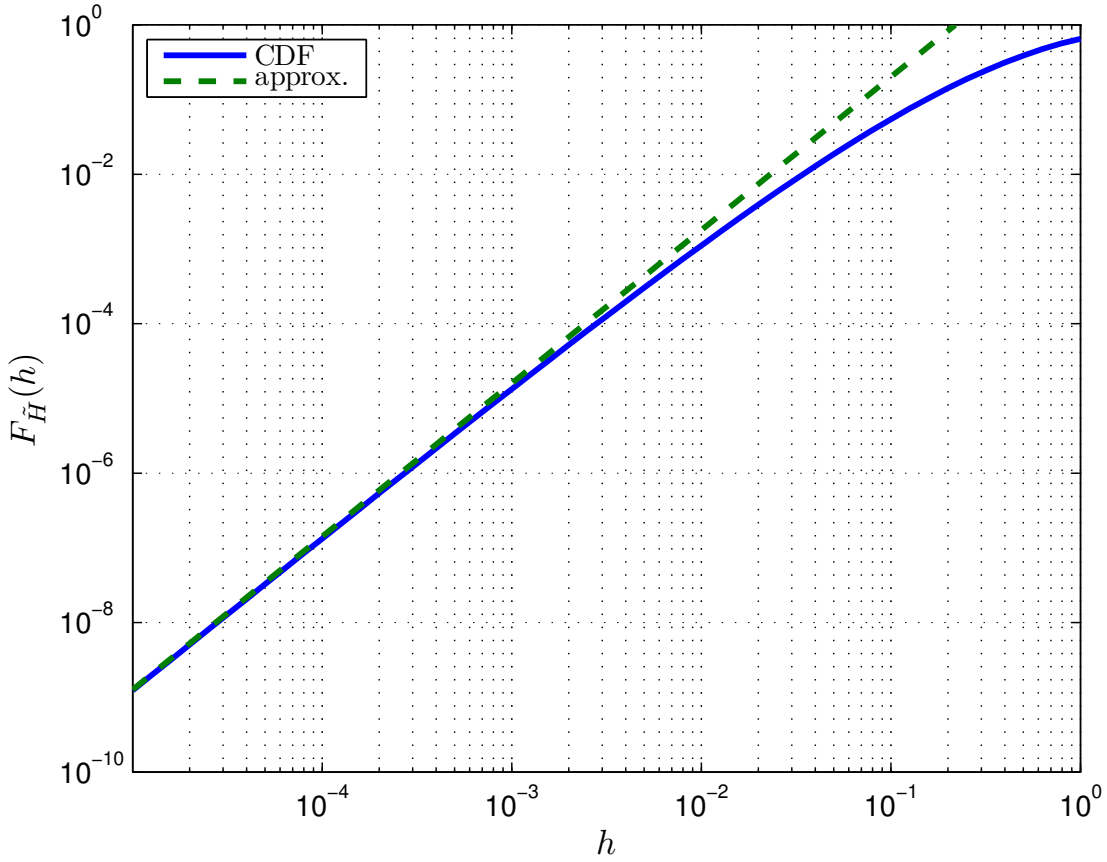

Fig. 5. Gamma-gamma cdf (30) (solid) and the approximation (31) (dashed) for $\alpha = 2.05$ and $\beta = 2.45$.

The parameter r is referred to as the *coherence parameter* [34], and is also well known as the Rice factor in the analysis of RF fading channels with a line of sight component. When $r = 0$, (32) becomes a Rayleigh pdf and the system reduces to the lognormal-exponential case. As $r \to \infty$ the pdf approaches a unit impulse function at $y = 1$. In other words as $r \to \infty$, $Y \to 1$, and the scintillation is purely lognormal distributed (weak turbulence case). Furthermore, as $r, \sigma \to 0$, the lognormal-Rice distribution reduces to the exponential distribution. Therefore, the lognormal-Rice distribution includes the lognormal, lognormal-exponential and exponential distributions as special cases.

The overall distribution of $\tilde{H} = XY$ has no closed form expression, but can be written in integral form [4]

$$f_{\tilde{H}}(h) = \frac{(1+r)e^{-r}}{\sqrt{2\pi}\sigma} \int_0^\infty \frac{1}{z^2} I_0\left(2\sqrt{\frac{(1+r)rh}{z}}\right) \exp\left(-\frac{(1+r)h}{z} - \frac{1}{2\sigma^2}\left(\log z + \frac{1}{2}\sigma^2\right)^2\right) dz \quad (35)$$

It is easy to show that for the scintillation distribution given by (35), the SI is given by

$$\sigma_I^2 = \exp(\sigma^2)\left(1 + \frac{1+2r}{(r+1)^2}\right) - 1. \quad (36)$$

Despite its complicated pdf, as will be shown later, we will still be able to determine the corresponding asymptotic outage probability behaviour in the general MIMO case.

IV. Outage Probability, Mutual Information and MMSE

The channel described by (7) under the quasi-static assumption is not information stable [44] and therefore, the channel capacity in the strict Shannon sense is zero. It can be shown that the codeword

error probability of any coding scheme can be lower bounded by the information outage probability [15, 16],

$$P_{\text{out}}(\mathsf{snr}, R) = \Pr(I(\boldsymbol{p}, \boldsymbol{h}) < R), \tag{37}$$

where R is the transmission rate and $I(\boldsymbol{p}, \boldsymbol{h})$ is the instantaneous input-output mutual information for a given power allocation $\boldsymbol{p} \triangleq (p_1, \ldots, p_B)$, and vector channel realisation $\boldsymbol{h} \triangleq (h_1, \ldots, h_B)$. The instantaneous mutual information can be expressed as [45]

$$I(\boldsymbol{p}, \boldsymbol{h}) = \frac{1}{B} \sum_{b=1}^{B} I^{\text{awgn}}(p_b h_b^2), \tag{38}$$

where $I^{\text{awgn}}(\rho)$ is the input-output mutual information of an AWGN channel with SNR ρ. For PPM [26]

$$I^{\text{awgn}}(\rho) = \log_2 Q - \mathbb{E}\left[\log_2\left(1 + \exp(-\rho) \sum_{q=2}^{Q} \exp\left(\sqrt{\rho}(Z_q - Z_1)\right)\right)\right], \tag{39}$$

where $Z_q \sim \mathcal{N}(0,1)$ for $q = 1, \ldots, Q$. We can show the following result.

Proposition 4.1: The input-output mutual information for Q-PPM transmission over an AWGN channel with SNR ρ can be lower bounded by

$$I^{\text{awgn}}(\rho) \geq I_{\text{lb}}^{\text{awgn}}(\rho) \triangleq \log_2 Q - \mathbb{E}_U\left[\log_2\left(1 + (Q-1)\exp\left(-\frac{\rho}{2} - \sqrt{\rho}U\right)\right)\right] \tag{40}$$

where $U \sim \mathcal{N}(0,1)$.

Proof: See Appendix III. ∎

Since $U \sim \mathcal{N}(0,1)$, the lower bound (40) can be efficiently computed using Gauss-Hermite quadratures [42]. Note that (40) was derived by [46] using the law of large numbers, and the authors considered it as an approximation. Here we proved that it is not just an approximation, but also a bound to the mutual information. Furthermore, as Q increases, $I^{\text{awgn}}(\rho) \to I_{\text{lb}}^{\text{awgn}}(\rho)$, i.e., $I_{\text{lb}}^{\text{awgn}}(\rho)$ is asymptotically tight for large Q. This can be observed in Fig 6, where the mutual information and the lower bound (40) are plotted for various values of Q. Remark that the bound (40) will lead to an upper bound to the outage probability.

For the CSIT case we will use the recently discovered relationship between mutual information and the MMSE [47]. This relationship states that[2]

$$\frac{d}{d\rho} I^{\text{awgn}}(\rho) = \frac{\mathsf{mmse}(\rho)}{\log(2)} \tag{41}$$

where $\mathsf{mmse}(\rho)$ is the MMSE in estimating the input from the output of a Gaussian channel as a function of the SNR ρ. For the case of PPM, we can express the MMSE as follows.

Theorem 4.1: Suppose QPPM symbols are transmitted across an AWGN channel with SNR ρ. Then, the MMSE is

$$\mathsf{mmse}(\rho) = 1 - \mathbb{E}\left[\frac{\exp(2\sqrt{\rho}(\sqrt{\rho} + Z_1)) + (Q-1)\exp(2\sqrt{\rho}Z_2)}{\left(\exp(\rho)\exp(\sqrt{\rho}Z_1) + \sum_{k=2}^{Q}\exp(\sqrt{\rho}Z_k)\right)^2}\right], \tag{42}$$

where $Z_i \sim \mathcal{N}(0,1)$ for $i = 1, \ldots, Q$.

Proof: See Appendix IV. ∎

A more careful look at the MMSE, yields the following result, which is relevant in the wideband regime [48].

[2]The $\log(2)$ term arises because we have defined $I^{\text{awgn}}(\rho)$ in bits/channel usage.

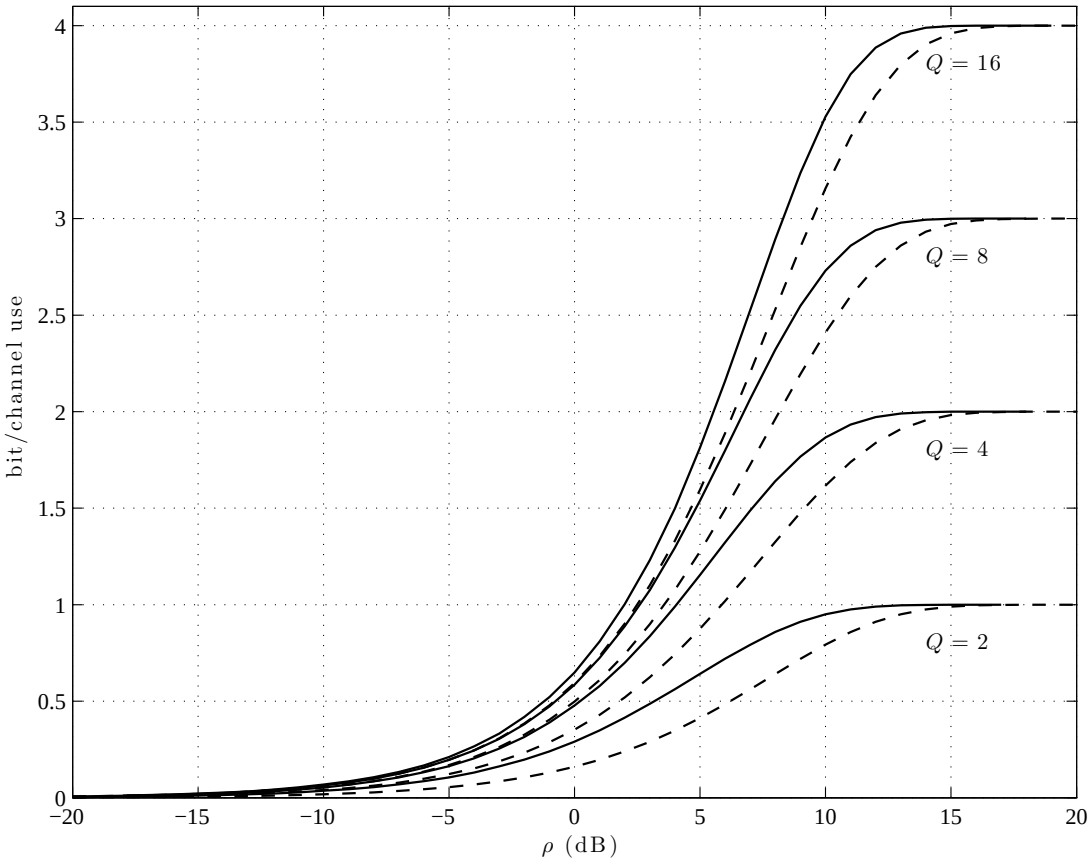

Fig. 6. Mutual information $I^{\mathrm{awgn}}(\rho)$ (solid lines) and lower bound $I_{\mathrm{lb}}^{\mathrm{awgn}}(\rho)$ (40) (dashed lines) for Q-PPM signal sets with $Q = 2, 4, 8, 16$.

Theorem 4.2:

$$\mathsf{mmse}(0) = \frac{Q-1}{Q} \tag{43}$$

Proof: See Appendix IV. ∎

Both (39) and (42) can be evaluated using standard Monte-Carlo methods.

Like the mutual information quantity (39), computation of (42) requires Q dimensional integration and we must again resort to Monte Carlo methods. Fig. 7 plots $\mathsf{mmse}(\rho)$ for increasing Q using this method.

V. Outage Probability Analysis with CSIR

For the CSIR case, we employ uniform power allocation, i.e. $p_1 = \ldots = p_B = \mathsf{snr}$. For codewords transmitted over B blocks, obtaining a closed form analytic expression for the outage probability is intractable. Even for $B = 1$, in some cases, for example the lognormal, gamma-gamma and lognormal-Rice distributions, determining the exact distribution of H can be a difficult task. Instead, as we shall see, obtaining the asymptotic behaviour of the outage probability is substantially simpler. Towards this end, and following the footsteps of [22, 49], we derive the *SNR exponent*.

Theorem 5.1: The outage SNR exponents for a MIMO FSO communications system modeled by (7)

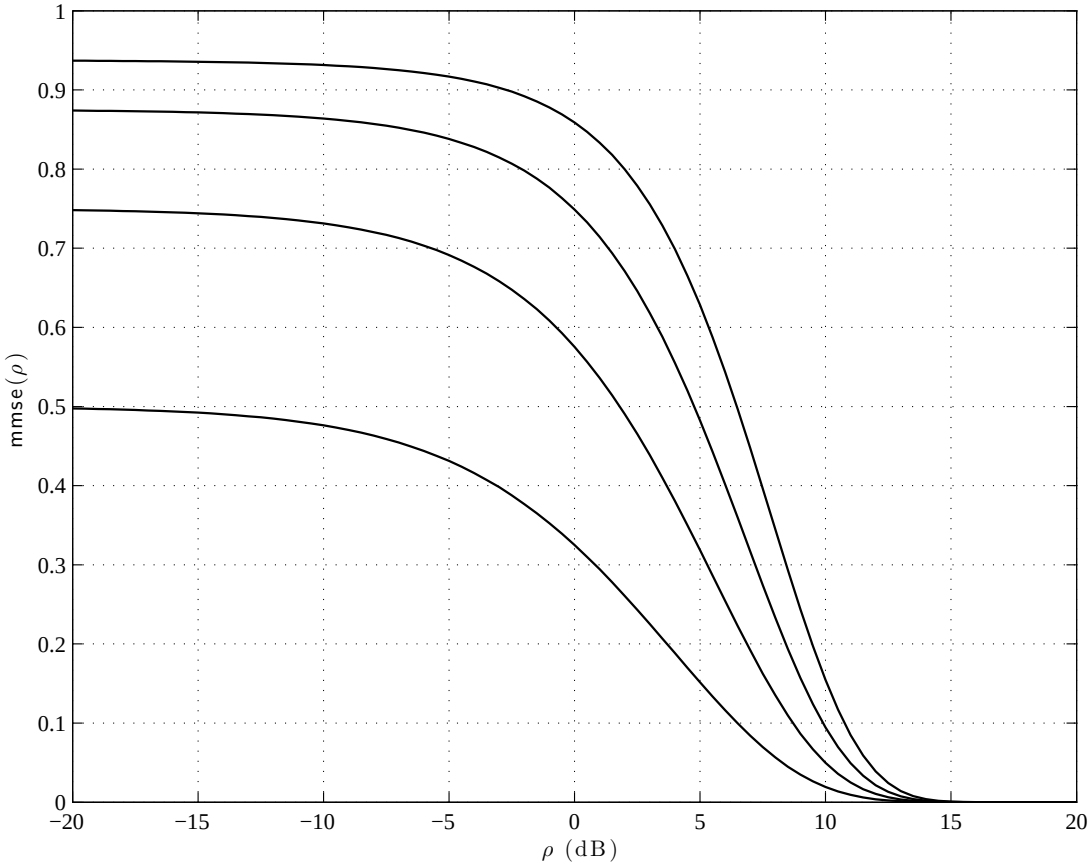

Fig. 7. Computation of $\mathsf{mmse}(\rho)$ (in dB) via Monte Carlo evaluation for $Q = 2, 4, 8, 16$. Larger Q corresponds to a higher $\mathsf{mmse}(\rho)$ curve.

are given as follows:

$$d^{\ln}_{(\log \mathsf{snr})^2} = \frac{MN}{8\log(1+\sigma_I^2)}\left(1 + \lfloor B\left(1-R_c\right)\rfloor\right) \tag{44}$$

$$d^{\exp}_{(\log \mathsf{snr})} = \frac{MN}{2}\left(1 + \lfloor B\left(1-R_c\right)\rfloor\right), \tag{45}$$

$$d^{\mathrm{gg}}_{(\log \mathsf{snr})} = \frac{MN}{2}\min(\alpha,\beta)\left(1 + \lfloor B\left(1-R_c\right)\rfloor\right), \tag{46}$$

$$d^{\mathrm{lr}}_{(\log \mathsf{snr})} = \frac{MN}{2}\left(1 + \lfloor B\left(1-R_c\right)\rfloor\right), \tag{47}$$

for lognormal, exponential, gamma-gamma and lognormal-Rice respectively, where $R_c = R/\log_2(Q)$ is the rate of the binary code and

$$d_{(\log \mathsf{snr})^k} \triangleq -\lim_{\mathsf{snr}\to\infty} \frac{\log P_{\mathrm{out}}(\mathsf{snr}, R)}{(\log \mathsf{snr})^k} \quad k = 1, 2. \tag{48}$$

Proof: See the Appendix. ■

Proposition 5.1: The outage SNR exponents for a MIMO FSO communications system modeled by (7) are given in Theorem 5.1, are achievable by random coding over PPM constellations whenever $B\left(1-R_c\right)$ is not an integer.

Proof: The proof follows from the proof of Theorem 5.1 and the proof of [22, Th. 1]. ■

The above results imply that the outage exponents given by (44)-(47) are the optimal SNR exponents over the channel: the outage probability is a lower bound to the error probability of any coding scheme, its corresponding exponents (given in Theorem 5.1) are an upper bound to the exponent of coding schemes.

From Proposition 5.1, we can achieve the outage exponents with a particular coding scheme (random coding, in this case), and therefore, the exponents given in Theorem 5.1 are optimal.

From (44)-(47) we immediately see the benefits of spatial and block diversity on the system. In particular, each exponent is proportional to: the number of lasers times the number of apertures, reflecting the spatial diversity; a channel related parameter that is dependent on the scintillation distribution; and the Singleton bound, which is the optimal rate-diversity tradeoff for Rayleigh-faded block fading channels [20–22].

Comparing the channel related parameters in (44)-(47) the effects of the scintillation distribution on the outage probability are directly visible. For the lognormal case, the channel related parameter is $8\log(1+\sigma_I^2)$ and hence is directly linked to the SI. Moreover, for small $\sigma_I^2 < 1$, $8\log(1+\sigma_I^2) \approx 8\sigma_I^2$ and the SNR exponent is inversely proportional to the SI. For the exponential case, the channel related parameter is a constant $1/2$ as expected, since the SI is constant. For the gamma-gamma case the channel related parameter is $\min(\alpha,\beta)/2$, which highlights an interesting connection between the outage probability and recent results in the theory of optical scintillation. For gamma-gamma distributed scintillation, the fading coefficient results from the product of two independent random variables, i.e. $\tilde{H} = XY$, where X and Y model fluctuations due to large scale and small scale cells. Large scale cells cause refractive effects that mainly distort the wave front of the propagating beam, and tend to steer the beam in a slightly different direction (i.e. beam wander). Small scale cells cause scattering by diffraction and therefore distort the amplitude of the wave through beam spreading and irradiance fluctuations [4, p. 160]. The parameters α, β are related to the large and small scale fluctuation variances via $\alpha = \sigma_X^{-2}$ and $\beta = \sigma_Y^{-2}$. For a plane wave (neglecting inner/outer scale effects) $\sigma_Y^2 > \sigma_X^2$, and as the strength of the optical turbulence increases, the small scale fluctuations dominate and $\sigma_Y^2 \to 1$ [4, p. 336]. This implies that the SNR exponent is exclusively dependent on the small scale fluctuations. Moreover, in the strong fluctuation regime, $\sigma_Y^2 \to 1$, the gamma-gamma distribution reduces to a K-distribution [4, p. 368], and the system has the same SNR exponent as the exponential case typically used to model very strong fluctuation regimes. In the case of lognormal-Rice scintillation, we observe that the exponent is exactly equal to that of exponential scintillation. Remark, however, that this does not imply that the two distributions yield the same outage probability. The inclusion of the Ricean component results in an error floor whose exponent is the same as that of the exponential distribution.

In comparing the lognormal exponent with the rest, we observe a striking difference. For the lognormal case (44) implies the outage probability is dominated by a $(\log(\mathsf{snr}))^2$ term, whereas for the other cases it is dominated by a $\log(\mathsf{snr})$ term. Thus the outage probability decays much more rapidly with SNR for the lognormal case than it does for the exponential or gamma-gamma cases. Furthermore, for the lognormal case, the slope of the outage probability curve, when plotted on a $\log$-$\log$ scale, will not converge to a constant value. In fact, a constant slope curve will only be observed when plotting the outage probability on a $\log$-$(\log)^2$ scale.

In deriving (44) (see Appendix V-A) we do not rely on the lognormal approximation, which has been used in e.g. [5, 12, 31] to simplify the analysis of FSO MIMO links in the presence of lognormal distributed scintillation. Under this approximation, we have an approximate exponent

$$d_{(\log \mathsf{snr})^2} \approx \frac{1}{8\log(1+\frac{\sigma_I^2}{MN})}\left(1+\lfloor B\left(1-R_c\right)\rfloor\right). \tag{49}$$

Comparing (44) and (49) we see that although the lognormal approximation also exhibits a $(\log(\mathsf{snr}))^2$ term, it has a different slope than the true SNR exponent. The difference is due to the lognormal approximation of the sum of random variables and the fact that the left tails of the true distribution and the approximation have different behaviours (see Fig. 2). However, for very small σ_I^2, using the approximation $\log(1+x) \approx x$ in (44) and (49) we see that they are approximately equal. This behaviour is shown in Fig. 8, which also shows that as σ_I^2 increases, the lognormal approximation (49) tends to underestimate the SNR exponent and worsens as MN increases.

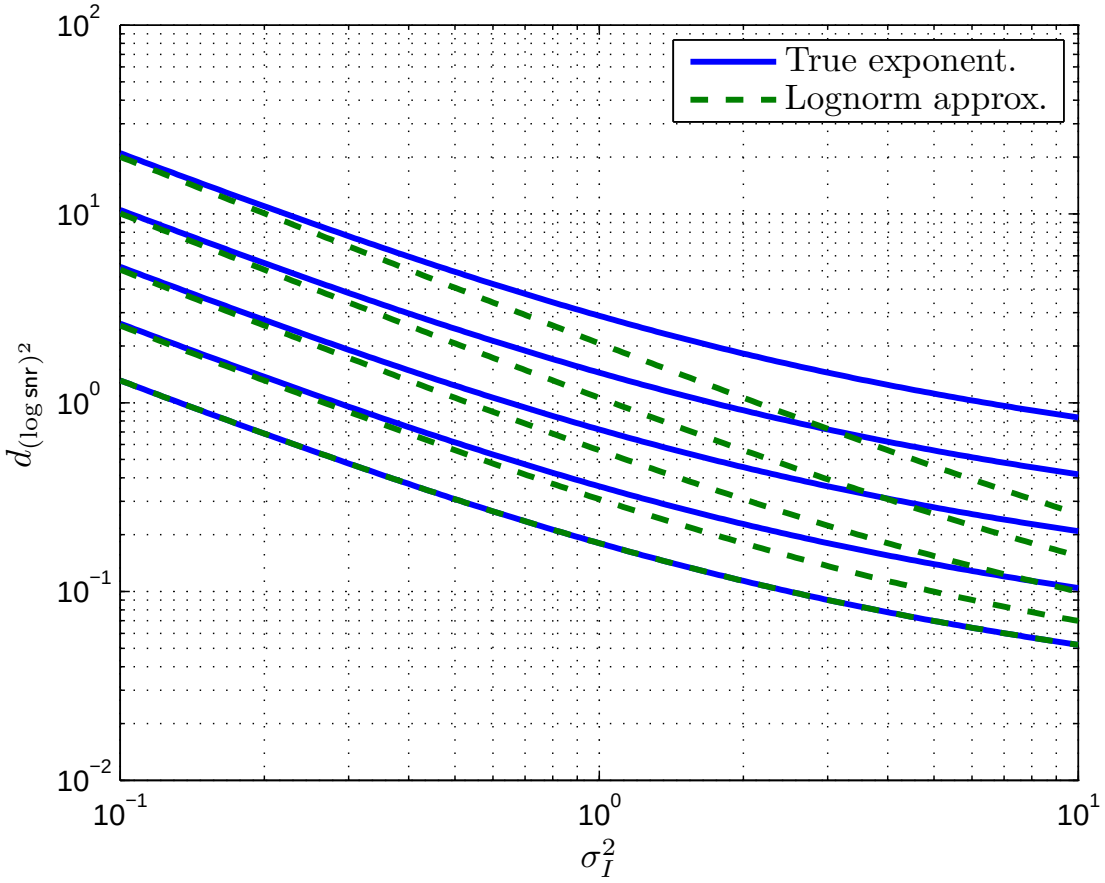

Fig. 8. Comparison of the SNR exponent (44) (solid) to the lognormal approximation (49) (dashed) for $B = 1$, $Q = 2$, $\mathsf{snr}_{1/2}^{\mathrm{awgn}} = 3.18$ dB and $MN = 1, 2, 4, 8, 16$ (highest curve pair corresponds to $MN = 16$).

For the special case of single block transmission, $B = 1$, it is straightforward to express the outage probability in terms of the cumulative distribution function (cdf) of the scintillation random variable, i.e.

$$P_{\mathrm{out}}(\mathsf{snr}, R) = F_H\left(\sqrt{\frac{\mathsf{snr}_R^{\mathrm{awgn}}}{\mathsf{snr}}}\right) \tag{50}$$

where $F_H(h)$ denotes the cdf of H, and $\mathsf{snr}_R^{\mathrm{awgn}} \triangleq I^{\mathrm{awgn},-1}(R)$ denotes the SNR value at which the mutual information is equal to R. Table I reports these values for $Q = 2, 4, 8, 16$ and $R = R_c \log_2 Q$, with $R_c = \frac{1}{4}, \frac{1}{2}, \frac{3}{4}$. Therefore, for $B = 1$, we can compute the outage probability analytically when the distribution of H is available, i.e., in the exponential case for $M, N \geq 1$ or in the lognormal and gamma-gamma cases for $M, N = 1$. In the case of exponential scintillation we have that

$$P_{\mathrm{out}}(\mathsf{snr}, R) = \bar{\Gamma}\left(MN, \left(MN(1+MN)\frac{\mathsf{snr}_R^{\mathrm{awgn}}}{\mathsf{snr}}\right)^{\frac{1}{2}}\right), \tag{51}$$

where $\bar{\Gamma}(a, x) \triangleq \frac{1}{\Gamma(a)} \int_0^x t^{a-1} \exp(-t)\, dt$ denotes the regularised (lower) incomplete gamma function [42, p.260]. As mentioned in Section III and described in the Appendix I, it is possible to evaluate the distribution numerically using the FFT, yielding very accurate computations of the outage probability for $B = 1$ and $M, N \geq 1$ in only a few seconds.

Outage probability curves for the $B = 1$ case are shown in Fig. 9. For the lognormal case, we see that the curves do not have constant slope for large SNR, while, for the exponential and gamma-gamma cases, a constant slope is clearly visible. In the case of lognormal-Rice scintillation, we observe that for

TABLE I

MINIMUM SIGNAL-TO-NOISE RATIO $\mathsf{snr}_R^{\mathrm{awgn}}$ (IN DECIBELS) FOR RELIABLE COMMUNICATION FOR TARGET RATE $R = R_c \log_2 Q$.

Q	$R_c = \frac{1}{4}$	$R_c = \frac{1}{2}$	$R_c = \frac{3}{4}$
2	-0.7992	3.1821	6.4109
4	0.2169	4.0598	7.0773
8	1.1579	4.8382	7.7222
16	1.9881	5.5401	8.3107

low SNR the behaviour is very close to the lognormal case, while at large SNR the curve changes slope and shows an error floor. The slope of the error floor is the same as the exponential curve as predicted by our analysis. We also see the benefits of MIMO, particularly in the exponential, gamma-gamma and lognormal-Rice cases, where the SNR exponent has increased from $1/2$ and 1 to 2 and 4 respectively. In the case of lognormal-Rice scintillation, we observe that the curve is very close to the lognormal one in the range of error probability shown in the figure. This curve will change slope, yielding an error floor parallel to that of the exponential case. To verify this, Figure 10 shows the outage probability for lognormal-Rice scintillation in a different range of error probability. As we observe, the error probability changes slope and shows an error floor of slope $MN/2 = 2$, as predicted by our analysis.

VI. OUTAGE PROBABILITY ANALYSIS WITH CSIT

In this section we consider the case where the transmitter and receiver both have perfect CSI knowledge. In this case, the transmitter determines the optimal power allocation that minimises the outage probability for a fixed rate, subject to a power constraint [23]. The results of this section are based on the application of results from [24] to PPM and the scintillation distributions of interest. Using these results we show power savings on the order of 20 dB with respect to the CSIR-only case, and uncover new insight as to how key design parameters influence the performance of the system.

For the short-term power constraint given by (9), the optimal power allocation is given by mercury-waterfilling at each channel realisation [24, 50],

$$p_b = \frac{1}{h_b^2}\mathsf{mmse}^{-1}\left(\min\left\{1, \frac{\eta}{h_b^2}\right\}\right), \tag{52}$$

for $b = 1, \ldots, B$ where $\mathsf{mmse}^{-1}(u)$ is the inverse-MMSE function and η is chosen to satisfy the power constraint. From [24, Prop. 1] it is apparent that the SNR exponent for the CSIT case under short-term power constraints is the same as the CSIR case.

For the long-term power constraint given by (10) the optimal power allocation is [24]

$$\boldsymbol{p} = \begin{cases} \boldsymbol{\wp}, & \sum_{b=1}^{B} \wp_b \leq s \\ \mathbf{0}, & \text{otherwise,} \end{cases} \tag{53}$$

where

$$\wp_b = \frac{1}{h_b^2}\mathsf{mmse}^{-1}\left(\min\left\{1, \frac{1}{\eta h_b^2}\right\}\right), \; b = 1, \ldots, B \tag{54}$$

and s is a threshold such that $s = \infty$ if $\lim_{s\to\infty} \mathbb{E}_{\mathcal{R}(s)}\left[\frac{1}{B}\sum_{b=1}^{B} \wp_b\right] \leq P$, and

$$\mathcal{R}(s) \triangleq \left\{\boldsymbol{h} \in \mathbb{R}_+^B : \frac{1}{B}\sum_{b=1}^{B} \wp_b \leq s\right\}, \tag{55}$$

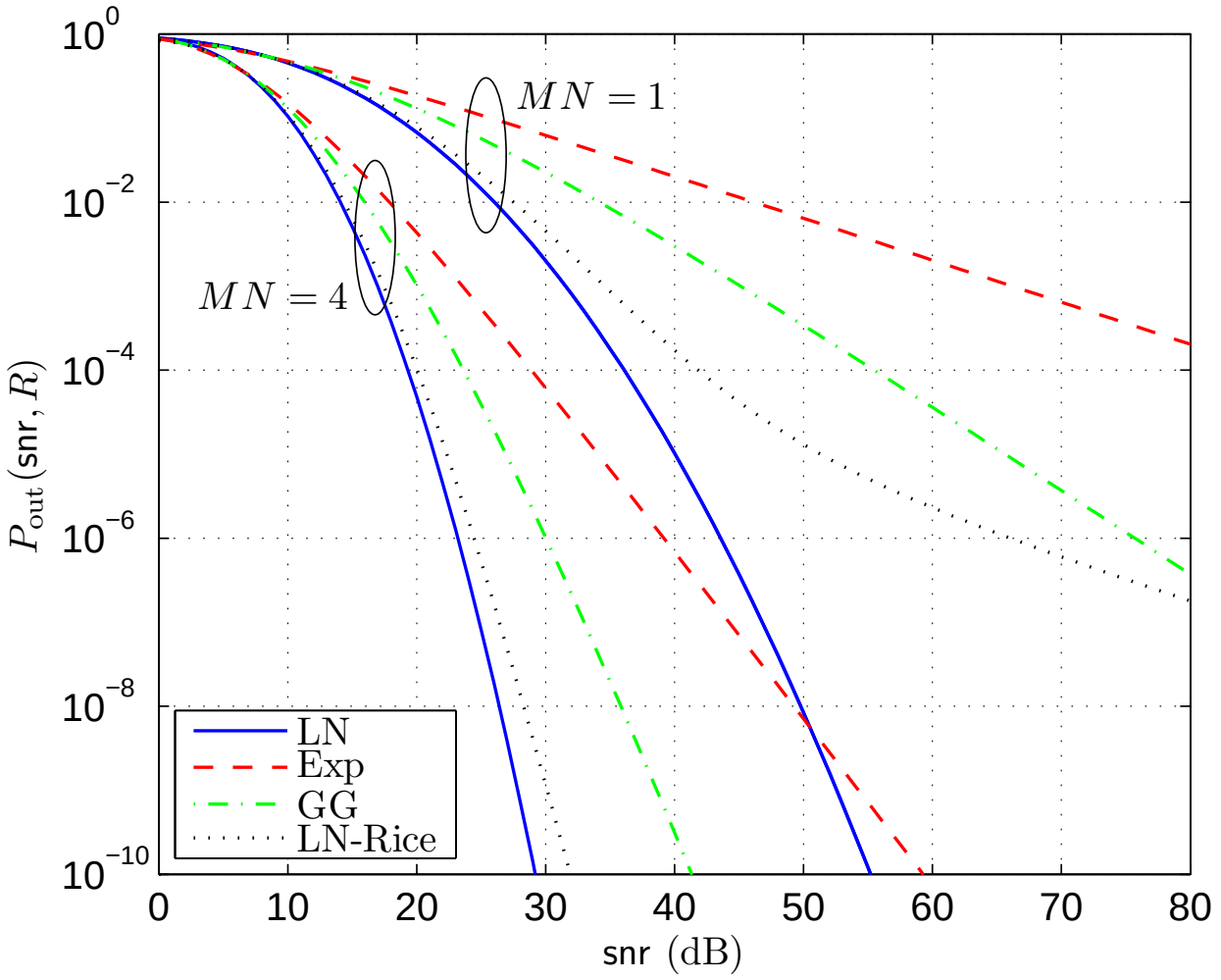

Fig. 9. Outage probability for lognormal (solid), exponential distributed (dashed), gamma-gamma distributed scintillation (dot-dashed) and lognormal-Rice (dotted) with $\sigma_I^2 = 1$, $\alpha = 2$, $\beta = 3$ (for gamma-gamma scintillation), $\sigma = 0.7301$ and $r = 10$ (for lognormal-Rice scintillation) $B = 1$, $Q = 2$, $R_c = 1/2$, $\mathsf{snr}_{1/2}^{\text{awgn}} = 3.18$ dB.

otherwise, s is chosen such that $P = \mathbb{E}_{\mathcal{R}(s)}\left[\frac{1}{B}\sum_{b=1}^{B} \wp_b\right]$. In (54), η is now chosen to satisfy the rate constraint

$$\frac{1}{B}\sum_{b=1}^{B} I^{\text{awgn}}\left(\mathsf{mmse}^{-1}\left(\min\left\{1, \frac{1}{\eta h_b^2}\right\}\right)\right) = R \tag{56}$$

From [24], the long-term SNR exponent is given by

$$d^{\text{lt}}_{(\log \mathsf{snr})} = \begin{cases} \frac{d^{\text{st}}_{(\log \mathsf{snr})}}{1 - d^{\text{st}}_{(\log \mathsf{snr})}} & d^{\text{st}}_{(\log \mathsf{snr})} < 1 \\ \infty & d^{\text{st}}_{(\log \mathsf{snr})} > 1 \end{cases}, \tag{57}$$

where $d^{\text{st}}_{(\log \mathsf{snr})}$ is the short-term SNR exponent, i.e., the SNR exponent obtained in the previous section. Note that $d^{\text{lt}}_{(\log \mathsf{snr})} = \infty$ implies the outage probability curve is vertical, i.e. delay-limited capacity [25] exists. From (44) we see that $d^{\text{st}}_{(\log \mathsf{snr})} = \infty$ for the lognormal case, i.e. delay-limited capacity always exists, and the outage probability curve is vertical. In the exponential and lognormal-Rice case from (45) and (47) we require that $MN\left(1 + \lfloor B\left(1 - R_c\right)\rfloor\right) > 2$, while in the gamma-gamma case from (46) we need $MN \min(\alpha, \beta)\left(1 + \lfloor B\left(1 - R_c\right)\rfloor\right) > 2$, for delay-limited capacity to exist. In other words, for these cases, M, N, B and R_c need to be chosen carefully to ensure the existance of delay-limited capacity.

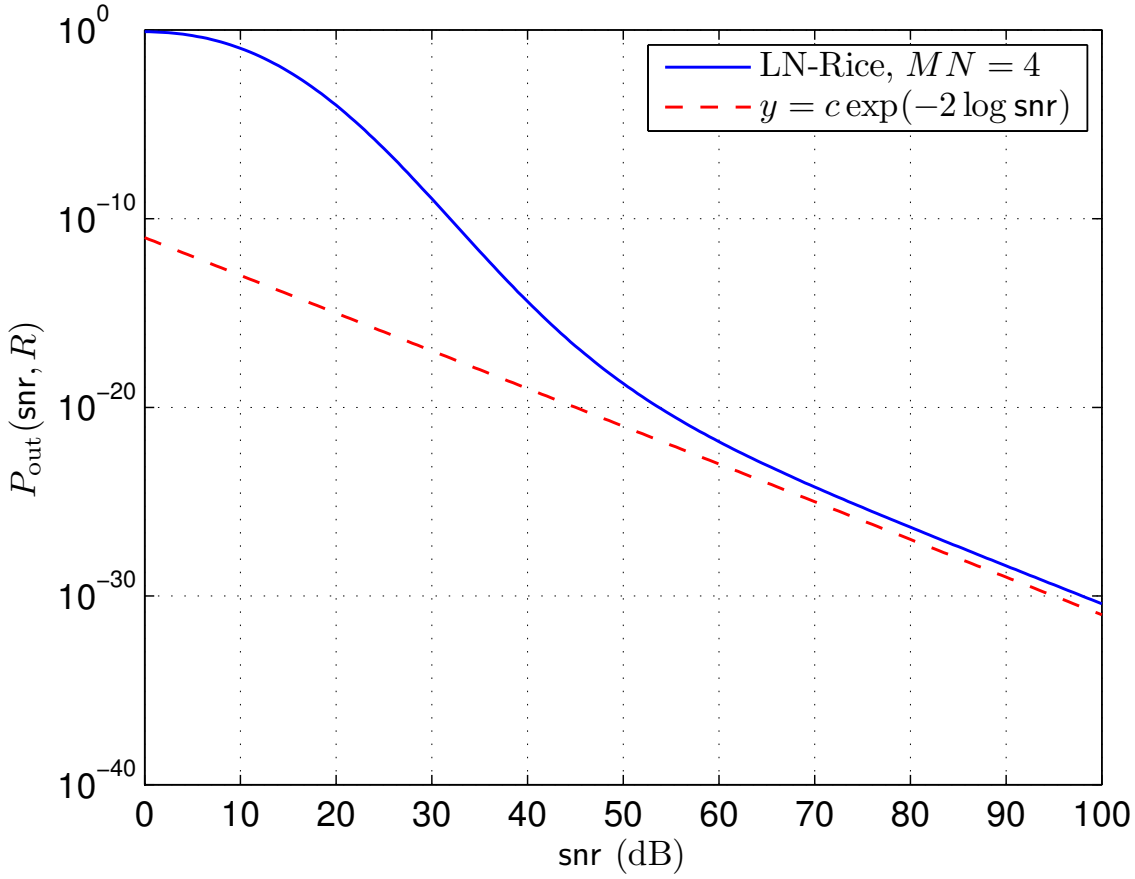

Fig. 10. Outage probability for lognormal-Rice with $\sigma_I^2 = 1$, $\sigma = 0.7301$ and $r = 10$ $B = 1$, $MN = 4$, $Q = 2$, $R_c = 1/2$, $\mathsf{snr}_{1/2}^{\text{awgn}} = 3.18$ dB.

Single block transmission ($B = 1$) is most relevant in FSO communications since the coherence time is on the order of milliseconds which is large compared to typical data rates. In this case the solution (54) can be determined explicitly since

$$\eta = \left(h^2 \mathsf{mmse}(I^{\text{awgn},-1}(R))\right)^{-1} = \left(h^2 \mathsf{mmse}(\mathsf{snr}_R^{\text{awgn}})\right)^{-1}. \tag{58}$$

Therefore,

$$\wp^{\text{opt}} = \frac{\mathsf{snr}_R^{\text{awgn}}}{h^2}. \tag{59}$$

Intuitively, (59) implies that for single block transmission, whenever $\mathsf{snr}_R^{\text{awgn}}/h^2 \leq s$, one simply transmits at the minimum power necessary so that the received instantaneous SNR is equal to the SNR threshold ($\mathsf{snr}_R^{\text{awgn}}$) of the code. Otherwise, transmission is turned off. Thus an outage occurs whenever $h < \sqrt{\frac{\mathsf{snr}_R^{\text{awgn}}}{s}}$ and hence

$$P_{\text{out}}(\mathsf{snr}, R) = F_H\left(\sqrt{\frac{\mathsf{snr}_R^{\text{awgn}}}{\gamma^{-1}(\mathsf{snr})}}\right) \tag{60}$$

where $\gamma^{-1}(\mathsf{snr})$ is the solution to the equation $\gamma(s) = \mathsf{snr}$, i.e.,

$$\gamma(s) = \mathsf{snr}_R^{\text{awgn}} \int_{\nu}^{\infty} \frac{f_H(h)}{h^2}\, dh, \tag{61}$$

where $\nu \triangleq \sqrt{\frac{\mathsf{snr}_R^{\mathrm{awgn}}}{s}}$. In the cases where the distribution of H is known in closed form, Eq. (61) can be solved explicitly, hence yielding the exact outage probability expression when combined with (60). For lognormal distributed scintillation and $B = M = N = 1$, the integral (59) can be solved explicitly,

$$\gamma^{\mathrm{ln}}(s) = \frac{1}{2}\mathsf{snr}_R^{\mathrm{awgn}}(1+\sigma_I^2)^4 \mathrm{erfc}\left(\frac{3\log(1+\sigma_I^2) + \frac{1}{2}\log \mathsf{snr}^{\mathrm{awgn}} - \frac{1}{2}\log s}{\sqrt{2\log(1+\sigma_I^2)}}\right). \tag{62}$$

We also find that

$$\lim_{s\to\infty} \mathsf{snr}^{\mathrm{ln}}(s) = \mathsf{snr}_R^{\mathrm{awgn}}(1+\sigma_I^2)^4, \tag{63}$$

which is precisely the threshold SNR at which $P_{\mathrm{out}}(\mathsf{snr}, R) \to 0$. For exponential distributed scintillation with $B = 1$, we obtain,

$$\gamma^{\mathrm{exp}}(s) = \mathsf{snr}_R^{\mathrm{awgn}} \frac{MN(1+MN)}{(MN-1)(MN-2)}\ \bar{\Gamma}\left(MN-2, \sqrt{MN(1+MN)\frac{\mathsf{snr}_R^{\mathrm{awgn}}}{s}}\right). \tag{64}$$

Similarly, for the case when $MN > 2$,

$$\lim_{s\to\infty} \mathsf{snr}^{\mathrm{exp}}(s) = \mathsf{snr}_R^{\mathrm{awgn}} \frac{MN(1+MN)}{(MN-1)(MN-2)}. \tag{65}$$

For the case when $MN \leq 2$, there exists no threshold SNR for which $P_{\mathrm{out}}(\mathsf{snr}, R) \to 0$. This is interesting, because it means that a combined total of more than 3 lasers and apertures is required to drive $P_{\mathrm{out}}(\mathsf{snr}, R) \to 0$ under strong turbulence conditions, unlike the weak turbulence case (lognormal), where a threshold s exists for any MN to drive $P_{\mathrm{out}}(\mathsf{snr}, R) \to 0$.

Fig. 11 compares the outage probability for the $B = 1$ CSIT case (with long-term power constraints) for each of the scintillation distributions. For the $MN = 1$ case we see that delay-limited capacity only exists in the lognormal case, since for the other two distributions $d^{\mathrm{st}}_{(\log \mathsf{snr})} < 1$. In this situation, one must code over more blocks to ensure the existance of delay-limited capacity. When $MN = 4$, delay-limited capacity exists in all three distribution cases since $d^{\mathrm{st}}_{(\log \mathsf{snr})} > 1$. Note that the SNR threshold at which $P_{\mathrm{out}} \to 0$ can be determined by computing the expectation $\mathsf{snr}_R^{\mathrm{awgn}}\mathbb{E}\left[H^{-2}\right]$, which, as described above, can be determined explicitly for some cases. Comparing the CSIR and CSIT cases (Figs. 9 and 11) we can see that very large power savings are possible when CSI is known at the transmitter. For example, for the case of gamma-gamma scintillation, at 10^{-4} we observe around 20 dB gain with power control (for $MN = 4$).

VII. Conclusions

In this report we have analysed the outage probability of the MIMO Gaussian FSO channel under the assumption of PPM and non-ideal PD, for lognormal, exponential, gamma-gamma and lognormal-Rice distributed scintillation. When CSI is known only at the receiver, we have shown that the SNR exponent is proportional to the number lasers and apertures, times a channel related parameter (dependent on the scintillation distribution), times the Singleton bound, even in the cases where a closed form expression of the equivalent SISO channel distribution is not available in closed-form. When the scintillation is lognormal distributed, we have shown that the outage probability is dominated by a $(\log(\mathsf{snr}))^2$ term, whereas for the exponential, gamma-gamma and lognormal-Rice cases it is dominated by a $\log(\mathsf{snr})$ term. When CSI is also known at the transmitter, we applied the power control techniques of [24] to PPM to show very significant power savings.

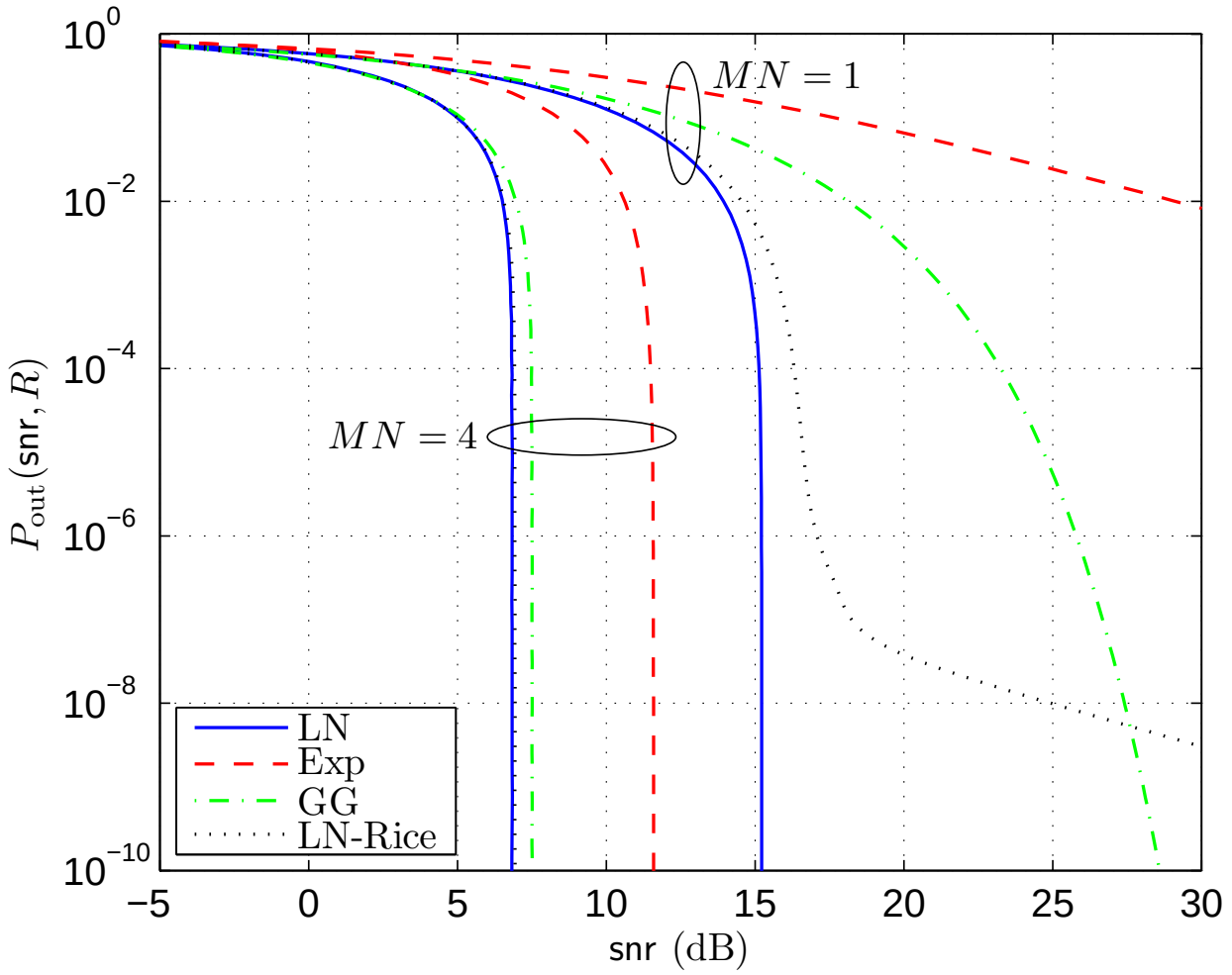

Fig. 11. Comparison of CSIR and CSIT outage probabilities for lognormal (solid), exponential (dashed), gamma-gamma (dash-dotted) and lognormal-Rice (dotted) distributed scintillation with $\sigma_I^2 = 1$, $\alpha = 2$, $\beta = 3$ (for gamma-gamma scintillation), $\sigma = 0.7301$ and $r = 10$ (for lognormal-Rice scintillation), $B = 1$, $Q = 2$, $\text{snr}_{1/2}^{\text{awgn}} = 3.18$ dB.

APPENDIX I
FAST FOURIER TRANSFORM METHOD

This appendix describes how to use the fast Fourier transform (FFT) to numerically compute the distribution of sums of i.i.d. random variables.

1) Set $\Delta_h = \frac{h_{\max}}{N_{\text{FFT}}}$, where $h_{\max}$ and N_{FFT} are the truncation value and FFT length respectively.
2) Compute $\phi[n] = cMN f_{\tilde{H}}(cMN\Delta_h n)$ for $n = 0, \ldots, N_{\text{FFT}} - 1$, where $c = \sqrt{\mathbb{E}[\hat{H}^2]}$ is given by (12).
3) Approximate the characteristic function via the discrete Fourier transform (DFT), i.e.

$$\Phi[k] = \Delta_h \sum_{n=0}^{N_{\text{FFT}}-1} \phi[n] \exp(-j2\pi kn/N_{\text{FFT}}) \tag{66}$$

for $k = 0 \ldots, N_{\text{FFT}} - 1$, which can be computed efficiently using an FFT algorithm.

4) Now compute the distribution by performing the inverse DFT (using an IFFT algorithm) as follows,

$$f_H(\Delta_h n) = \frac{1}{\Delta_h} \frac{1}{N_{\text{FFT}}} \sum_{k=0}^{N_{\text{FFT}}-1} (\Phi[k])^{MN} \exp(j2\pi kn/N_{\text{FFT}}), \tag{67}$$

for $n = 0 \ldots, N_{\text{FFT}} - 1$.

APPENDIX II
GAMMA-GAMMA DISTRIBUTION PROOFS

A. Proof of Theorem 3.1

We begin using the property that the Gamma-Gamma distributed random variable can be written as the product of two independent Gamma distributed random variables X and Y, i.e. $p_X(x) = g(x; \alpha, 1/\alpha)$ and $p_X(y) = g(y; \beta, 1/\beta)$ where $g(k, \theta)$ is defined as in (20). Hence we have

$$\begin{aligned}
M_h(t) &= \mathbb{E}[\exp(tXY)] \\
&= \int_0^\infty \int_0^\infty \exp(txy) g(x; \alpha, 1/\alpha) g(y; \beta, 1/\beta)\, dxdy \\
&= \int_0^\infty \left(1 - \frac{t}{\alpha} y\right)^{-\alpha} g(y; \beta, 1/\beta)\, dy \qquad (68) \\
&= \sum_i^\infty \binom{\alpha + i - 1}{i} \left(\frac{t}{\alpha}\right)^i \int_0^\infty y^i g(y; \beta, 1/\beta)\, dy \qquad (69) \\
&= \sum_{i=0}^\infty \frac{\Gamma(\alpha + i)}{\Gamma(\alpha) i!} \left(\frac{t}{\alpha}\right)^i \frac{\Gamma(\beta + i)}{\Gamma(\beta)\beta^i} \\
&= \sum_{i=0}^\infty \frac{(\alpha)_i (\beta)_i}{i!} \left(\frac{t}{\alpha\beta}\right)^i \\
&= {}_2\mathrm{F}_0(\alpha, \beta; t/(\alpha\beta)),
\end{aligned}$$

where in (68) we used the MGF of a Gamma distributed random variable and in (69) we used the Binomial theorem.

B. Proof of Proposition 3.1

For small h the gamma-gamma pdf can be approximated as

$$f_{\tilde{H}}(h) \approx \begin{cases} \frac{2\alpha^{2\alpha}}{(\Gamma(\alpha))^2} h^{\alpha-1} \log \frac{1}{2\alpha\sqrt{h}}, & \beta = \alpha \\ \frac{\Gamma(|\alpha-\beta|)}{\Gamma(\alpha)\Gamma(\beta)} (\alpha\beta h)^{\min(\alpha,\beta)-1}, & \beta \neq \alpha \end{cases},$$

where we have used $\mathrm{K}_0(x) \sim -\log(x)$ and $\mathrm{K}_\nu(x) \sim \frac{1}{2}\Gamma(\nu)\left(\frac{2}{x}\right)^\nu$ for $\nu > 0$ and $x \to 0$ [42, p. 375]. The result therefore follows via simple integration.

APPENDIX III
PROOF OF PROPOSITION 4.1

Using Jensen's inequality [45] we have that

$$I^{\mathrm{awgn}}(\rho) = \log_2 Q - \mathbb{E}_{\mathbf{y}|\mathbf{x}=\mathbf{e}_1}\left[\log_2\left(1+\sum_{q=2}^{Q}\exp\left(\sqrt{\rho}(y_q-y_1)\right)\right)\right] \tag{70}$$

$$\geq \log_2 Q - \mathbb{E}_{y_1|\mathbf{x}=\mathbf{e}_1}\left[\log_2\left(1+\sum_{q=2}^{Q}\mathbb{E}_{y_q|\mathbf{x}=\mathbf{e}_1}\left[\exp\left(\sqrt{\rho}(y_q-y_1)\right)\right]\right)\right] \tag{71}$$

$$= \log_2 Q - \mathbb{E}_{y_1|\mathbf{x}=\mathbf{e}_1}\left[\log_2\left(1+\exp(-\sqrt{\rho}y_1)\sum_{q=2}^{Q}\mathbb{E}_{y_q|\mathbf{x}=\mathbf{e}_1}\left[\exp\left(\sqrt{\rho}y_q\right)\right]\right)\right] \tag{72}$$

$$= \log_2 Q - \mathbb{E}_{y_1|\mathbf{x}=\mathbf{e}_1}\left[\log_2\left(1+(Q-1)\exp(-\sqrt{\rho}y_1)\exp\left(\frac{\rho}{2}\right)\right)\right] \tag{73}$$

$$= \log_2 Q - \mathbb{E}_{U}\left[\log_2\left(1+(Q-1)\exp(-\sqrt{\rho}(\sqrt{\rho}+U))\exp\left(\frac{\rho}{2}\right)\right)\right] \tag{74}$$

$$= \log_2 Q - \mathbb{E}_{U}\left[\log_2\left(1+(Q-1)\exp\left(-\frac{\rho}{2}-\sqrt{\rho}U\right)\right)\right] \tag{75}$$

where (73) follows from $y_q \sim \mathcal{N}(0,1)$ for $q = 2,\ldots,Q$, which implies that $\exp(\sqrt{\rho}y_q)$ is lognormal with mean $\exp\left(\frac{\rho}{2}\right)$.

APPENDIX IV
PROOF OF THEOREM 4.1

The MMSE estimate is given by

$$\hat{\boldsymbol{x}} = \mathbb{E}\left[\boldsymbol{x}|\boldsymbol{y}\right] \tag{76}$$

$$= \sum_{\boldsymbol{x}\in\mathcal{X}} \boldsymbol{x} p(\boldsymbol{x}|\boldsymbol{y}) \tag{77}$$

$$= \sum_{\boldsymbol{x}\in\mathcal{X}} \frac{\boldsymbol{x} p(\boldsymbol{y}|\boldsymbol{x}) p(\boldsymbol{x})}{p(\boldsymbol{y})} \tag{78}$$

$$= \sum_{\boldsymbol{x}\in\mathcal{X}} \frac{\boldsymbol{x} p(\boldsymbol{y}|\boldsymbol{x}) p(\boldsymbol{x})}{\sum_{\boldsymbol{x}'\in\mathcal{X}} p(\boldsymbol{y}|\boldsymbol{x}') p(\boldsymbol{x}')} \tag{79}$$

$$= \sum_{\boldsymbol{x}\in\mathcal{X}} \frac{\boldsymbol{x} p(\boldsymbol{y}|\boldsymbol{x})}{\sum_{\boldsymbol{x}'\in\mathcal{X}} p(\boldsymbol{y}|\boldsymbol{x}')} \tag{80}$$

$$= \sum_{\boldsymbol{x}\in\mathcal{X}} \frac{\boldsymbol{x} \exp\left(-\frac{1}{2}\|\boldsymbol{y} - \sqrt{\rho}\boldsymbol{x}\|^2\right)}{\sum_{\boldsymbol{x}'\in\mathcal{X}} \exp\left(-\frac{1}{2}\|\boldsymbol{y} - \sqrt{\rho}\boldsymbol{x}'\|^2\right)}, \tag{81}$$

$$= \sum_{q=1}^{Q} \frac{\boldsymbol{e}_q \exp(\sqrt{\rho} y_q)}{\sum_{i=1}^{Q} \exp(\sqrt{\rho} y_i)} \tag{82}$$

where (76)-(77) follow from the definition of the MMSE estimate [51], (78) is application of Bayes' rule, (80) assumes equiprobable input symbols and (81) follows since $\boldsymbol{y}$ Gaussian conditioned on $\boldsymbol{x}$.

From (82) the ith element of $\hat{\boldsymbol{x}}$ is

$$\hat{x}_i = \frac{\exp(\sqrt{\rho} y_i)}{\sum_{k=1}^{Q} \exp(\sqrt{\rho} y_k)}. \tag{83}$$

Now, the MMSE is defined as [51]

$$\begin{aligned} \mathsf{mmse}(\rho) &= \mathbb{E}\left[\|\boldsymbol{x} - \hat{\boldsymbol{x}}\|^2\right] \\ &= \mathbb{E}[\|\boldsymbol{x}\|^2] - \mathrm{E}[\|\hat{\boldsymbol{x}}\|^2], \end{aligned} \tag{84}$$

where the last line follows from the *orthogonality principle* [51]. Now,

$$\mathbb{E}[\|\boldsymbol{x}\|^2] = \sum_{x\in\mathcal{X}} p(\boldsymbol{x})\|\boldsymbol{x}\|^2 = \sum_{x\in\mathcal{X}} \frac{1}{Q} = 1. \tag{85}$$

Due to the symmetry of QPPM we may assume that $\boldsymbol{x} = \boldsymbol{e}_1$ was transmitted. Hence, from (83),

$$\mathbb{E}[\|\hat{\boldsymbol{x}}\|^2] = \sum_{i=1}^{Q} \mathbb{E}[\hat{x}_i^2] \tag{86}$$

$$= \mathbb{E}[\hat{x}_1^2] + (Q-1)\mathbb{E}[\hat{x}_2^2] \tag{87}$$

Since $y_1 = \sqrt{\rho} + z_1$ and $y_i = z_i$ for $i = 2, \ldots, Q$ we may write

$$\mathbb{E}[\hat{x}_1^2] = \mathbb{E}\left[\frac{\exp(2\sqrt{\rho}(\sqrt{\rho} + z_1))}{\left(\exp(\sqrt{\rho}(\sqrt{\rho} + z_1)) + \sum_{k=2}^{Q} \exp(\sqrt{\rho} z_k)\right)^2}\right] \tag{88}$$

Similarly,

$$\mathbb{E}[\hat{x}_2^2] = \mathbb{E}\left[\frac{\exp(2\sqrt{\rho} z_2)}{\left(\exp(\rho)\exp(\sqrt{\rho} z_1) + \sum_{k=2}^{Q} \exp(\sqrt{\rho} z_k)\right)^2}\right]. \tag{89}$$

Hence combining (88), (88) and (84) the theorem follows.

PROOF OF THEOREM 4.2

The theorem follows directly from setting $\rho = 0$ in (81). We find that the estimate that minimizes the mean squared error is $\hat{\boldsymbol{x}} = (\frac{1}{Q}, \ldots, \frac{1}{Q})$. Regardless of which symbol was transmitted, the squared error is

$$\|\boldsymbol{x} - \hat{\boldsymbol{x}}\|^2 = \frac{Q-1}{Q^2} + \left(1 - \frac{1}{Q}\right)^2 = \frac{Q-1}{Q}.$$

Hence (43) follows.

APPENDIX V
PROOF OF THEOREM 5.1

We begin by defining a normalized (with respect to SNR) fading coefficient,

$$\zeta_b^{m,n} = -\frac{2\log \tilde{h}_b^{m,n}}{\log \mathsf{snr}}, \tag{90}$$

which has a pdf given by

$$f_{\zeta_b^{m,n}}(\zeta) = \frac{\log \mathsf{snr}}{2} \exp\left(-\frac{1}{2}\zeta \log \mathsf{snr}\right) f_{\tilde{H}}\left(\exp\left(-\frac{1}{2}\zeta \log \mathsf{snr}\right)\right). \tag{91}$$

Since we are only concerned with the asymptotic outage behaviour, the scaling of the coefficients is irrelevant, and to simplify our analysis we assume $\mathbb{E}[\hat{H}^2] = 1$. Hence the instantaneous SNR for block b is given by

$$\rho_b = \mathsf{snr} h_b^2 = \mathsf{snr}\left(\frac{1}{MN}\sum_{m=1}^{M}\sum_{n=1}^{N}\tilde{h}_b^{m,n}\right)^2 = \left(\frac{1}{MN}\sum_{m=1}^{M}\sum_{n=1}^{N}\mathsf{snr}^{\frac{1}{2}\left(1-\zeta_b^{m,n}\right)}\right)^2 \tag{92}$$

for $b = 1, \ldots, B$. Therefore,

$$\lim_{\mathsf{snr}\to\infty} I^{\text{awgn}}(\rho_b) = \lim_{\mathsf{snr}\to\infty} I^{\text{awgn}}\left(\left(\frac{1}{MN}\sum_{m=1}^{M}\sum_{n=1}^{N}\mathsf{snr}^{\frac{1}{2}\left(1-\zeta_b^{m,n}\right)}\right)^2\right) \tag{93}$$

$$= \begin{cases} 0 & \text{if all } \zeta_b^{m,n} > 1 \\ \log_2 Q & \text{at least one } \zeta_b^{m,n} < 1 \end{cases} \tag{94}$$

$$= \log_2 Q\left(1 - \mathbb{1}\{\boldsymbol{\zeta}_b \succ \mathbf{1}\}\right) \tag{95}$$

where $\boldsymbol{\zeta}_b \triangleq (\zeta_b^{1,1}, \ldots, \zeta_b^{M,N})$, $\mathbb{1}\{\cdot\}$ denotes the indicator function, $\mathbf{1} \triangleq (1, \ldots, 1)$ is a $1 \times MN$ vector of 1's, and the notation $\boldsymbol{a} \succ \boldsymbol{b}$ for vectors $\boldsymbol{a}, \boldsymbol{b} \in \mathbb{R}^k$ means that $a_i > b_i$ for $i = 1, \ldots, k$.

From the definition of outage probability (37), we have that[3]

$$P_{\text{out}}(\mathsf{snr}, R) = \Pr(I_{\boldsymbol{h}}(\mathsf{snr}) < R) \tag{96}$$

$$= \int_{\mathcal{A}} f(\boldsymbol{\zeta}) d\boldsymbol{\zeta} \tag{97}$$

where $\boldsymbol{\zeta} \triangleq (\boldsymbol{\zeta}_1, \ldots, \boldsymbol{\zeta}_B)$ is a $1 \times BMN$ vector of normalized fading coefficients, $f(\boldsymbol{\zeta})$ denotes their joint pdf, and

$$\mathcal{A} \triangleq \left\{\boldsymbol{\zeta} \in \mathbb{R}^{BMN} : \frac{1}{B}\sum_{b=1}^{B}\log_2 Q\left(1 - \mathbb{1}\{\boldsymbol{\zeta}_b \succ \mathbf{1}\}\right) < R\right\} \tag{98}$$

$$= \left\{\boldsymbol{\zeta} \in \mathbb{R}^{BMN} : \sum_{b=1}^{B}\mathbb{1}\{\boldsymbol{\zeta}_b \succ \mathbf{1}\} > B\left(1 - \frac{R}{\log_2 Q}\right)\right\} \tag{99}$$

is the asymptotic outage set. We now compute the asymptotic behaviour of the outage probability, i.e.

$$-\lim_{\mathsf{snr}\to\infty}\log P_{\text{out}}(\mathsf{snr}, R) = -\lim_{\mathsf{snr}\to\infty}\log\int_{\mathcal{A}} f(\boldsymbol{\zeta}) d\boldsymbol{\zeta}. \tag{100}$$

[3]Note we have dropped the suffix $\boldsymbol{p}$ in (37) since the power is uniformly allocated across all blocks (CSIR case).

A. Lognormal case

Suppose $\tilde{h}_b^{m,n}$ are lognormal distributed with parameters $\mu = -\log(1+\sigma_I^2)$ and $\sigma^2 = \log(1+\sigma_I^2)$ (see Sec. III). Hence, from (91) and (15) the pdf of $\zeta_b^{m,n}$ is

$$f_{\zeta_b^{m,n}}(\zeta) = \frac{\log \mathsf{snr}}{\sqrt{8\pi\sigma^2}} \exp\left(-\frac{1}{8\sigma^2}\left((\log \mathsf{snr})^2\zeta^2 + 4\mu \log \mathsf{snr}\zeta + 4\mu^2\right)\right) \tag{101}$$

$$\doteq \exp\left(-\frac{1}{8\sigma^2}(\log \mathsf{snr})^2\zeta^2\right). \tag{102}$$

Therefore the joint pdf of $\boldsymbol{\zeta}$ is,

$$f(\boldsymbol{\zeta}) = \frac{(\log \mathsf{snr})^{BMN}}{(8\pi\sigma^2)^{\frac{BMN}{2}}} \exp\left(-\frac{1}{8\sigma^2}\sum_{b=1}^{B}\sum_{m=1}^{M}\sum_{n=1}^{N}\left((\log \mathsf{snr})^2(\zeta_b^{m,n})^2 + 4\mu \log \mathsf{snr}\zeta_b^{m,n} + 4\mu^2\right)\right) \tag{103}$$

$$\doteq \exp\left(-\frac{(\log \mathsf{snr})^2}{8\sigma^2}\sum_{b=1}^{B}\sum_{m=1}^{M}\sum_{n=1}^{N}(\zeta_b^{m,n})^2\right). \tag{104}$$

Hence, from (100) we have

$$-\lim_{\mathsf{snr}\to\infty} \log P_{\text{out}}(\mathsf{snr}, R) = -\lim_{\mathsf{snr}\to\infty} \log \int_{\mathcal{A}} \exp\left(-\frac{(\log \mathsf{snr})^2}{8\sigma^2}\sum_{b=1}^{B}\sum_{m=1}^{M}\sum_{n=1}^{N}(\zeta_b^{m,n})^2\right) d\boldsymbol{\zeta}, \tag{105}$$

which using Varadhan's lemma [52] gives

$$-\lim_{\mathsf{snr}\to\infty} \log P_{\text{out}}(\mathsf{snr}, R) = \inf_{\mathcal{A}}\left\{\frac{(\log \mathsf{snr})^2}{8\sigma^2}\sum_{b=1}^{B}\sum_{m=1}^{M}\sum_{n=1}^{N}(\zeta_b^{m,n})^2\right\} \tag{106}$$

$$= \frac{(\log \mathsf{snr})^2}{8\sigma^2}\inf_{\mathcal{A}}\left\{\sum_{b=1}^{B}\sum_{m=1}^{M}\sum_{n=1}^{N}(\zeta_b^{m,n})^2\right\} \tag{107}$$

It is not difficult to show that [22]

$$\inf_{\mathcal{A}}\left\{\sum_{b=1}^{B}\sum_{m=1}^{M}\sum_{n=1}^{N}(\zeta_b^{m,n})^2\right\} = \kappa MN \tag{108}$$

where κ is the unique integer satisfying

$$\kappa < B\left(1 - \frac{R}{\log_2 Q}\right) \leq \kappa + 1. \tag{109}$$

Hence it follows that

$$-\lim_{\mathsf{snr}\to\infty} \log P_{\text{out}}(\mathsf{snr}, R) = (\log \mathsf{snr})^2 \ \frac{MN}{8\sigma^2}\left(1 + \left\lfloor B\left(1 - \frac{R}{\log_2 Q}\right)\right\rfloor\right), \tag{110}$$

and the SNR exponent is therefore

$$d_{(\log \mathsf{snr})^2} \triangleq -\lim_{\mathsf{snr}\to\infty} \frac{\log P_{\text{out}}(\mathsf{snr}, R)}{(\log \mathsf{snr})^2} = \frac{MN}{8\sigma^2}\left(1 + \left\lfloor B\left(1 - \frac{R}{\log_2 Q}\right)\right\rfloor\right) \tag{111}$$

$$= \frac{MN}{8\log(1+\sigma_I^2)}\left(1 + \left\lfloor B\left(1 - \frac{R}{\log_2 Q}\right)\right\rfloor\right). \tag{112}$$

which is a channel-related parameter times the Singleton bound [20–22].

B. Exponential case

The proof of this theorem follows the same arguments outlined in Appendix V-A. However, since we know the distribution of H explicitly, i.e. (23), our approach is even simpler. We begin by writing the distribution of $\zeta_b = -\frac{2\log h_b}{\log \mathsf{snr}}$ using (91) and (23), i.e.

$$f_{\zeta_b}(\zeta_b) = \log \mathsf{snr} \frac{(MN(1+MN))^{\frac{MN}{2}}}{2\Gamma(MN)} e^{-\frac{MN}{2}\zeta_b \log \mathsf{snr} - \exp\left(-\frac{\zeta_b}{2}\sqrt{MN(1+MN)}\log \mathsf{snr}\right)} \tag{113}$$

$$\doteq \frac{\log \mathsf{snr}}{2} \frac{(MN(1+MN))^{\frac{MN}{2}}}{\Gamma(MN)} \exp\left(-\frac{MN}{2}\zeta_b \log \mathsf{snr}\right), \quad \zeta_b > 0 \tag{114}$$

for large snr. Hence we obtain joint pdf,

$$f(\boldsymbol{\zeta}) = (\log \mathsf{snr})^B \frac{(MN(1+MN))^{\frac{BMN}{2}}}{(2\Gamma(MN))^B} e^{-\left(\log \mathsf{snr}\frac{MN}{2}\sum_{b=1}^B \zeta_b\right) - \left(\sum_{b=1}^B \exp\left(-\frac{\zeta_b}{2}\sqrt{MN(1+MN)}\log \mathsf{snr}\right)\right)} \tag{115}$$

$$\doteq (\log \mathsf{snr})^B \frac{(MN(1+MN))^{\frac{BMN}{2}}}{(2\Gamma(MN))^B} \exp\left(-\log \mathsf{snr}\frac{MN}{2}\sum_{b=1}^B \zeta_b\right) \tag{116}$$

Following the same steps in Appendix V-A, i.e. the defining the same asymptotic outage set and application of Varadhan's lemma [52], then we find that

$$-\lim_{\mathsf{snr}\to\infty} \log P_{\text{out}}(\mathsf{snr}, R) = \frac{MN}{2}\log \mathsf{snr}\left(1 + \left\lfloor B\left(1 - \frac{R}{\log_2 Q}\right)\right\rfloor\right),$$

and hence the SNR exponent is

$$d_{(\log \mathsf{snr})} \triangleq -\lim_{\mathsf{snr}\to\infty} \frac{\log P_{\text{out}}(\mathsf{snr}, R)}{\log \mathsf{snr}} = \frac{MN}{2}\left(1 + \left\lfloor B\left(1 - \frac{R}{\log_2 Q}\right)\right\rfloor\right).$$

as given in the statement of the theorem.

C. Gamma-gamma case

Suppose $\tilde{h}_b^{m,n}$ are gamma-gamma distributed with parameters α and β. Let us first assume $\alpha > \beta$. Using the general expression (91) we find that

$$f_{\zeta_b^{m,n}}(\zeta) = \log \mathsf{snr} \frac{(\alpha\beta)^{\frac{\alpha+\beta}{2}}}{\Gamma(\alpha)\Gamma(\beta)} \exp\left(-\frac{\alpha+\beta}{4}\zeta \log \mathsf{snr}\right) \mathrm{K}_{\alpha-\beta}\left(2\sqrt{\alpha\beta}\exp\left(-\frac{1}{4}\zeta \log \mathsf{snr}\right)\right)$$

$$\doteq \log \mathsf{snr} \frac{(\alpha\beta)^{\frac{\alpha+\beta}{2}}}{\Gamma(\alpha)\Gamma(\beta)} \frac{\Gamma(\alpha-\beta)}{2} \exp\left(-\frac{\beta}{2}\zeta \log \mathsf{snr}\right), \quad \zeta > 0 \tag{117}$$

for large snr, where we have used the approximation $\mathrm{K}_\nu(x) \approx \frac{1}{2}\Gamma(\nu)(\frac{1}{2}x)^{-\nu}$ for small x and $\nu > 0$ [42, p. 375]. The extra condition, $\zeta > 0$, is required to ensure the argument of the Bessel function approaches zero as $\mathsf{snr} \to \infty$ so that the aforementioned approximation can be employed. For the case $\beta > \alpha$ we need only swap α and β in (118). Hence we have

$$f_{\zeta_b^{m,n}}(\zeta) \doteq \log \mathsf{snr} \frac{(\alpha\beta)^{\frac{\alpha+\beta}{2}}}{\Gamma(\alpha)\Gamma(\beta)} \frac{\Gamma(|\alpha-\beta|)}{2} \exp\left(-\frac{\min(\alpha,\beta)}{2}\zeta \log \mathsf{snr}\right). \tag{118}$$

For B blocks, M inputs and N outputs we therefore have that the joint pdf,

$$f(\boldsymbol{\zeta}) \doteq \exp\left(-\frac{\min(\alpha,\beta)\log \mathsf{snr}}{2}\sum_{b=1}^B\sum_{m=1}^M\sum_{n=1}^N \zeta_b^{m,n}\right), \quad \boldsymbol{\zeta} \succ \mathbf{0}. \tag{119}$$

Now, following the same steps as in the lognormal case, with the additional constraint $\boldsymbol{\zeta}_b \succ \mathbf{0}$, we find that

$$d_{(\log \mathsf{snr})} = \frac{\min(\alpha,\beta)MN}{2}\left(1+\left\lfloor B\left(1-\frac{R}{\log_2 Q}\right)\right\rfloor\right),$$

as given in the statement of the theorem.

Alternatively, the theorem can also be proved without requiring the gamma-gamma pdf explicitly. This involves considering $\tilde{h}_b^{m,n} = x_b^{m,n} y_b^{m,n}$, where $x_b^{m,n}$ and $y_b^{m,n}$ are independent gamma random variables distributed according to $g(x;\alpha,1/\alpha)$ and $g(y;\beta,1/\beta)$ respectively (see (20)). Then defining normalized coefficients $\zeta_b^{m,n} = -\frac{2\log x_b^{m,n}}{\log \mathsf{snr}}$ and $\xi_b^{m,n} = -\frac{2\log y_b^{m,n}}{\log \mathsf{snr}}$ and the instantaneous SNR,

$$\rho_b = \frac{1}{MN}\sum_{m=1}^{M}\sum_{n=1}^{N} \mathsf{snr}^{1-\frac{1}{2}(\zeta_b^{m,n}+\xi_b^{m,n})}. \tag{120}$$

Hence,

$$\lim_{\mathsf{snr}\to\infty} I^{\text{awgn}}(\rho_b) = \log_2 Q\left(1-\mathbb{1}\left\{\frac{1}{2}(\boldsymbol{\zeta}_b+\boldsymbol{\xi}_b)\succ \mathbf{1}\right\}\right). \tag{121}$$

Therefore,

$$P_{\text{out}}(\mathsf{snr},R) = \int_{\mathcal{A}} f(\boldsymbol{\zeta},\boldsymbol{\xi})\, d\boldsymbol{\zeta}\, d\boldsymbol{\xi} \tag{122}$$

where

$$\mathcal{A} \triangleq \left\{\boldsymbol{\zeta}\in\mathbb{R}^{BMN}, \boldsymbol{\xi}\in\mathbb{R}^{BMN} : \sum_{b=1}^{B}\mathbb{1}\left\{\frac{1}{2}(\boldsymbol{\zeta}_b+\boldsymbol{\xi}_b)\succ\mathbf{1}\right\} > B\left(1-\frac{R}{\log_2 Q}\right)\right\} \tag{123}$$

is the asymptotic outage set. From (20) and (91) we find that,

$$f_{\zeta_b^{m,n}}(\zeta) \doteq \exp\left(-\frac{\alpha}{2}\zeta\log\mathsf{snr}\right) \tag{124}$$

$$f_{\xi_b^{m,n}}(\xi) \doteq \exp\left(-\frac{\beta}{2}\xi\log\mathsf{snr}\right). \tag{125}$$

Hence the joint pdf of $(\boldsymbol{\zeta},\boldsymbol{\xi})$ is

$$f(\boldsymbol{\zeta},\boldsymbol{\xi}) \doteq \exp\left(-\frac{1}{2}\log\mathsf{snr}\sum_{b=1}^{B}\sum_{m=1}^{M}\sum_{n=1}^{N}\alpha\zeta_b^{m,n}+\beta\xi_b^{m,n}\right). \tag{126}$$

Thus using, Varadhan's lemma [52]

$$-\lim_{\mathsf{snr}\to\infty}\log P_{\text{out}}(\mathsf{snr},R) = \frac{1}{2}\log\mathsf{snr}\inf_{\mathcal{A}}\left\{\sum_{b=1}^{B}\sum_{m=1}^{M}\sum_{n=1}^{N}\alpha\zeta_b^{m,n}+\beta\xi_b^{m,n}\right\}. \tag{127}$$

To solve the above infimum, first suppose $\alpha>\beta$, then we set $\boldsymbol{\zeta}_b=\mathbf{0}$ for all $b=1,\ldots,B$ and assign any κ (where κ is defined in (109)) of the B vectors $\boldsymbol{\xi}_b$, $b=1,\ldots,B$, to be vectors such that $\frac{1}{2}\boldsymbol{\xi}_b\succ\mathbf{1}$, and the remaining $B-\kappa$ vectors to be $\mathbf{0}$. For the case when $\beta>\alpha$ we need only reverse the roles of $\boldsymbol{\zeta}_b$ and $\boldsymbol{\xi}_b$. Thus,

$$\inf_{\mathcal{A}}\left\{\sum_{b=1}^{B}\sum_{m=1}^{M}\sum_{n=1}^{N}\alpha\zeta_b^{m,n}+\beta\xi_b^{m,n}\right\} = \min(\alpha,\beta)MN\kappa, \tag{128}$$

and it therefore follows that

$$d_{(\log \mathsf{snr})} = \frac{\min(\alpha,\beta)MN}{2}\left(1+\left\lfloor B\left(1-\frac{R}{\log_2 Q}\right)\right\rfloor\right).$$

D. Lognormal-Rice Distribution

For this case, $\tilde{H} = XY$, where X and $\sqrt{Y}$ are lognormal and Rice distributed random variables respectively. To obtain the SNR exponent we follow the steps of the gamma-gamma case and define normalized fading coefficients, $\zeta_b^{m,n}$ and $\xi_b^{m,n}$.

From (101) (keeping $(\log \mathsf{snr})^2$ and $\log \mathsf{snr}$ terms),

$$f_{\zeta_b^{m,n}}(\zeta) \doteq \exp\left(-\frac{1}{8\sigma^2}(\log \mathsf{snr})^2\zeta^2 + \frac{1}{2}\zeta \log \mathsf{snr}\right). \tag{129}$$

From (34),

$$\begin{aligned} f_{\xi_b^{m,n}}(\xi) =& \frac{r+1}{2}\log \mathsf{snr} \exp\left(-\frac{1}{2}\xi \log \mathsf{snr} - r - (r+1)\exp\left(-\frac{1}{2}\xi \log \mathsf{snr}\right)\right) \\ & \cdot I_0\left(\sqrt{4r(r+1)\exp\left(-\frac{1}{2}\xi \log \mathsf{snr}\right)}\right), \end{aligned}$$

and using $I_0(z) \to 1$ as $z \to 0$ [42, p. 376] we find that

$$f_{\xi_b^{m,n}}(\xi) \doteq \exp\left(-\frac{1}{2}\xi \log \mathsf{snr}\right). \tag{130}$$

Hence we have,

$$f(\boldsymbol{\zeta}, \boldsymbol{\xi}) \doteq \exp\left(-\frac{1}{8\sigma^2}(\log \mathsf{snr})^2 \sum_{b=1}^{B}\sum_{m=1}^{M}\sum_{n=1}^{N}(\zeta_b^{m,n})^2 - \frac{1}{2}\log \mathsf{snr} \sum_{b=1}^{B}\sum_{m=1}^{M}\sum_{n=1}^{N}(\xi_b^{m,n} - \zeta_b^{m,n})\right), \tag{131}$$

and using, Varadhan's lemma [52]

$$\begin{aligned} & -\lim_{\mathsf{snr}\to\infty} \log P_{\text{out}}(\mathsf{snr}, R) \\ & \qquad = \frac{1}{2}\log \mathsf{snr} \inf_{\mathcal{A}} \left\{ \frac{1}{4\sigma^2}\log \mathsf{snr} \sum_{b=1}^{B}\sum_{m=1}^{M}\sum_{n=1}^{N}(\zeta_b^{m,n})^2 + \sum_{b=1}^{B}\sum_{m=1}^{M}\sum_{n=1}^{N}(\xi_b^{m,n} - \zeta_b^{m,n}) \right\}, \end{aligned} \tag{132}$$

where $\mathcal{A}$ is given by (123). Assuming $\sigma^2 < \infty$, immediately we see that the above infimum is achieved by setting $\boldsymbol{\zeta}_b = \mathbf{0}$ and the $\boldsymbol{\xi}_b$ vectors as in the gamma-gamma case. Hence the SNR exponent is

$$d_{(\log \mathsf{snr})} = \frac{MN}{2}\left(1 + \left\lfloor B\left(1 - \frac{R}{\log_2 Q}\right)\right\rfloor\right).$$

REFERENCES

[1] H. Willebrand and B. S. Ghuman, *Free-Space Optics: Enabling Optical Connectivity in Today's Networks*, Sams Publishing, Indianapolis, USA, 2002.

[2] J. W. Strohbehn, Ed., *Laser Beam Propagation in the Atmosphere*, vol. 25, Springer-Verlag, Germany, 1978.

[3] R. M. Gagliardi and S. Karp, *Optical communications*, John Wiley & Sons, Inc., Canada, 1995.

[4] L. C. Andrews and R. L. Phillips, *Laser Beam Propagation through Random Media*, SPIE Press, USA, 2nd edition, 2005.

[5] N. Letzepis, I. Holland, and W. Cowley, "The Gaussian free space optical MIMO channel with Q-ary pulse position modulation," *to appear IEEE Trans. Wireless Commun.*, 2008.

[6] K. Chakraborty, S. Dey, and M. Franceschetti, "On outage capacity of MIMO Poisson fading channels," in *Proc. IEEE Int. Symp. Inform. Theory*, July 2007.

[7] K. Chakraborty and P. Narayan, "The Poisson fading channel," *IEEE Trans. Inform. Theory*, vol. 53, no. 7, pp. 2349–2364, July 2007.

[8] N. Cvijetic, S. G. Wilson, and M. Brandt-Pearce, "Receiver optimization in turbulent free-space optical MIMO channels with APDs and Q-ary PPM," *IEEE Photon. Tech. Let.*, vol. 19, no. 2, pp. 103–105, Jan. 2007.

[9] I. B. Djordjevic, B. Vasic, and M. A. Neifeld, "Multilevel coding in free-space optical MIMO transmission with q-ary PPM over the atmospheric turbulence channel," *IEEE Photon. Tech. Let.*, vol. 18, no. 14, pp. 1491–1493, July 2006.

[10] S. G. Wilson, M. Brandt-Pearce, Q. Cao, and J. H. Leveque, "Free-space optical MIMO transmission with Q-ary PPM," *IEEE Trans. on Commun.*, vol. 53, no. 8, pp. 1402–1412, Aug. 2005.

[11] K. Chakraborty, "Capacity of the MIMO optical fading channel," in *Proc. IEEE Int. Symp. Inform. Theory*, Adelaide, Sept. 2005, pp. 530–534.

[12] E. J. Lee and V. W. S. Chan, "Part 1: optical communication over the clear turbulent atmospheric channel using diversity," *J. Select. Areas Commun.*, vol. 22, no. 9, pp. 1896–1906, Nov. 2005.

[13] S. M. Haas and J. H. Shapiro, "Capacity of wireless optical communications," *IEEE J. Select. Areas Commun.*, vol. 21, no. 8, pp. 1346–1356, Oct. 2003.

[14] A. A. Farid and S. Hranilovic, "Outage capacity optimization for free-space optical links with pointing errors," *IEEE Trans. Light. Tech.*, vol. 25, no. 7, pp. 1702–1710, July 2007.

[15] L. H. Ozarow, S. Shamai and A. D. Wyner, "Information theoretic considerations for cellular mobile radio," *IEEE Trans. on Vehicular Tech.*, vol. 43, no. 2, pp. 359–378, May 1994.

[16] E. Biglieri, J. Proakis and S. Shamai, "Fading channels: information-theoretic and communications aspects," *IEEE Trans. on Inform. Theory*, vol. 44, no. 6, pp. 2619 –2692, Oct. 1998.

[17] M. A. Al-Habash, L. C. Andrews, and R. L. Phillips, "Mathematical model for the irradiance probability density function of a laser beam propagating through turbulent media," *SPIE Opt. Eng.*, vol. 40, no. 8, pp. 1554–1562, 2001.

[18] J. H. Churnside and R. G. Frehlich, "Experimental evaluation of log-normally modulated rician and IK models of optical scintillation in the atmosphere," *J. Opt. Soc. Am. A*, vol. 6, no. 11, pp. 1760–1766, 1989.

[19] R. J. Hill and R. G. Frehlich, "Probability distribution of irradiance for the onset of strong scintillation," *J. Opt. Soc. Am. A*, vol. 14, no. 7, pp. 1530–1540, July 1997.

[20] R. Knopp and P. Humblet, "On coding for block fading channels," *IEEE Trans. on Inform. Theory*, vol. 46, no. 1, pp. 1643–1646, July 1999.

[21] E. Malkamaki and H. Leib, "Coded diversity on block-fading channels," *IEEE Trans. on Inform. Theory*, vol. 45, no. 2, pp. 771–781, March 1999.

[22] A. Guillén i Fàbregas and G. Caire, "Coded modulation in the block-fading channel: Coding theorems and code construction," *IEEE Trans. on Information Theory*, vol. 52, no. 1, pp. 262–271, Jan. 2006.

[23] G. Caire, G. Taricco and E. Biglieri, "Optimum power control over fading channels," *IEEE Trans. on Inform. Theory*, vol. 45, no. 5, pp. 1468–1489, July 1999.

[24] K. D. Nguyen, A. Guillén i Fàbregas, and L. K. Rasmussen, "Power allocation for discrete-input delay-limied fading channels," *submitted to IEEE Trans. Inf. Theory.,* `http://arxiv.org/abs/0706.2033`, Jun. 2007.

[25] S. V. Hanly and D. N. C. Tse, "Multiaccess fading channels. II. delay-limited capacities," *IEEE Trans. on Inform. Theory*, vol. 44, no. 7, pp. 2816–2831, Nov. 1998.

[26] S. Dolinar, D. Divsalar, J. Hamkins, and F. Pollara, "Capacity of pulse-position modulation (PPM) on Gaussian and Webb channels," *JPL TMO Progress Report 42-142*, Aug. 2000, URL: lasers.jpl.nasa.gov/PAPERS/OSA/142h.pdf.

[27] S. Dolinar, D. Divsalar, J. Hamkins, and F. Pollara, "Capacity of PPM on APD-detected optical channels," in *21st Cent. Millitary Commun. Conf. Proc.*, Oct. 2000, vol. 2, pp. 876–880.

[28] X. Zhu and J. M. Kahn, "Performance bounds for coded free-space optical communications through atmospheric turbulence channels," *IEEE Trans. on Commun.*, vol. 51, no. 8, pp. 1233–1239, Aug. 2003.

[29] J. Li and M. Uyasl, "Optical wireless communications: system model, capacity and coding," in *IEEE 58th Vehicular Tech. Conf.*, Oct. 2003, vol. 1, pp. 168–172.

[30] M. K. Simon and V. A. Vilnrotter, "Alamouti-type space-time coding for free-space optical communication with direct detection," *IEEE Trans. Wireless Commun.*, , no. 1, pp. 35–39, Jan 2005.

[31] S. M. Navidpour, M. Uysal, and M. Kavehrad, "BER performance of free-space optical transmission with spatial diversity," *IEEE Trans. on Wireless Commun.*, vol. 6, no. 8, pp. 2813–2819, August 2007.

[32] L. C. Andrews, R. L. Phillips, C. Y. Hopen, and M. A. Al-Habash, "Theory of optical scintillation," *J. Opt. Soc. Am. A*, vol. 16, no. 6, pp. 1417–1429, June 1999.

[33] R. S. Lawrence and J. W. Strohbehn, "A survey of clean-air propagation effects relevant to optical communications," *Proc. IEEE*, vol. 58, no. 10, pp. 1523–1545, Oct. 1970.

[34] J. H. Churnside and S. F. Clifford, "Log-normal Rician probability-density function of optical scintillations in the turbulent atmosphere," *J. Opt. Soc. Am. A*, vol. 4, no. 10, pp. 1923–1930, Oct. 1987.

[35] F. S. Vetelino, C. Young, L. Andrews, and J. Recolons, "Aperture averaging effects on the probability density of irrandiance fluctuations in moderate-to-strong turbulence," *Applied Optics*, vol. 46, no. 11, pp. 2099–2108, April 2007.

[36] P. Beckmann, *Probability in Communication Engineering*, Harcourt, Brace and World, New York, 1967.

[37] R. L. Mitchell, "Permanence of the log-normal distribution," *J. Opt. Soc. Am.*, 1968.

[38] S. B. Slimane, "Bounds on the distribution of a sum of independent lognormal random variables," *IEEE Trans. on Commun.*, vol. 49, no. 6, pp. 975–978, June 2001.

[39] N. C. Beaulieu and X. Qiong, "An optimal lognormal approximation to lognormal sum distributions," *IEEE Trans. Vehic. Tech.*, vol. 53, no. 2, March 2004.

[40] N. C. Beaulieu and F. Rajwani, "Highly accurate simple closed-form approximations to lognormal sum distributions and densities," *IEEE Commun. Let.*, vol. 8, no. 12, pp. 709–711, Dec. 2004.

[41] N. L. Johnson and S. Kotz, *Continuous univariate distributions - 1*, John Wiley & Sons, USA, 1970.

[42] M. Abramowitz and I. A. Stegun, *Handbook of Mathematical Functions with Formulas, Graphs and Mathematical Tables*, New York: Dover Press, 1972.

[43] A. Papoulis, *Probability, random variables, and stochastic processes*, McGraw-Hill, 1991.

[44] S. Verdú and T. S. Han, "A general formula for channel capacity," *IEEE Trans. on Inform. Theory*, vol. 40, no. 4, pp. 1147–1157, Jul. 1994.

[45] T. M. Cover and J. A. Thomas, *Elements of Information Theory*, Wiley Series in Telecommunications, 1991.

[46] S. Dolinar, D. Divsalar, J. Hamkins, and F. Pollara, "Capacity of pulse-position modulation (ppm) on gaussian and webb channels," *NASA JPL TMO Progress Report 42-142*, August 2000.

[47] D. Guo, S. Shamai, and S. Verdú, "Mutual information and minimum mean-square error in Gaussian channels," *IEEE Trans. Inf. Theory*, vol. 51, no. 4, pp. 1261–1282, Apr. 2005.

[48] S. Verdú, "Spectral efficiency in the wideband regime," *IEEE Trans. Inf. Theory*, vol. 48, no. 6, pp. 1319–1343, Jun. 2002.

[49] L. Zheng and D. Tse, "Diversity and multiplexing: A fundamental tradeoff in multiple antenna channels," *IEEE Trans. on Inform. Theory*, vol. 49, no. 5, May 2003.

[50] A. Lozano, A. M. Tulino, and S. Verdú, "Optimum power allocation for parallel Gaussian channels with arbitrary input distributions," *IEEE Trans. Inform. Theory*, vol. 52, no. 7, pp. 3033–3051, July 2006.

[51] S. M. Kay, *Fundamentals of Statistical Signal Processing: Estimation Theory*, Prentice Hall Int. Inc., USA, 1993.

[52] A. Dembo and O. Zeitouni, *Large Deviations Techniques and Applications*, Number 38 in Applications of Mathematics. Springer Verlag, 2nd edition, April 1998.